MASTERS THESIS

Modeling spatial inhomogeneities in solar cells

Effects of spatial microscopic defects on luminescence intensity

Author:
Ismail KAAYA

Supervisors:
Laurent LOMBEZ
Daniel ORY

Department of Physics
ECOLE POLYTECHNIQUE (UNIVERSITE PARIS SACLAY)

A dissertation submitted to the University of Paris Saclay in accordance with the requirements of the degree of MASTERS in the Faculty of Physics.

SEPTEMBER 2016

Abstract

Microscopic spatial defects (inhomogeneities) in solar cells have a detrimental impact on the overall performance of the solar cells. These defects can be due to the polycrystalline nature of the photovoltaic absorber (general case) or on the other hand, the characterization method itself can induce such inhomogeneities (ex: local excitation with confocal system). Photoluminescence imaging in particular is the most attractive type of experimental characterization technique which has been studied by many research groups. Since it is contactless, it allows a complete analysis of the photovoltaic material and it can actually be performed at each step of the solar cell fabrication process. To properly analyze the recorded images, one has to model the transport properties. In this work we model the transport properties in 2D using both a numerical and analytic approach. First,we model the global illumination of the sample, we then analyze the effects of grains and surface recombination. Second, we study lateral transport that can be influenced by recombination at the surface (passivation issues), grain boundaries (polycrystalline cells) or local artifacts (shunts, defects...). At the same time we are able to extract the lifetime knowing the generation rate and solving the excess carrier density from our model. And finally we implement our model to extract some cell parameters like the diffusion length from experimental data through data fitting.

Acknowledgments

He has not thanked God who has not thanked people." First, I would like to thank both my tutors Laurent Lombez and Daniel Ory for their insight and mentorship, and for creating a collaborative and congenial working atmosphere for me during all the process of my internship. I thank them also for their time in reviewing my report, I am very grateful for that.
Special thanks also goes to Dac-Trung Nguyen, postdoc fellow and IRDEP and Jerome Michallon, Posdoc fellow at LPN, for your precious help in MATLAB and mathematical problems, you really did a great work for the successful completion of my modeling part.
I cannot forget to thank everyone at IRDEP especially those who were attending the Monday meetings, you are a brilliant group of scientists, I really enjoyed listening to everyone's ideas, comments and discussions. This made my stay at IRDEP very fruitful because apart from my own research topic, I got a chance to learn about what other people are doing, this widened my knowledge in the PV field. This six months period has really been a time of tremendous learning and growth for me both scientifically and personally.
Lastly I extend my thanks to TOTAL who provided me with a scholarship and took part in the REST masters program at Ecole polytechnique. I am really very grateful.

Dedication

To my daddy Mr. Nsubuga and my siblings.

I am indebted to all of you for your love, support and encouragement through everything. I could not have done it without you.
Thank you.

Kaaya Ismail
Ecole polytechnique
September 2016

AUTHOR'S DECLARATION

I KAAYA Ismail, declare that this thesis titled, 'Modeling spatial inhomogeneities in thin film solar cells' and the work presented in it is my own. I confirm that this work submitted for assessment is my own and is expressed in my own words. Any uses made within it of the works of other authors in any form (e.g., ideas, equations, figures, text,tables, programs) are properly acknowledged at any point of their use. A list of the references employed is included.

SIGNED: ..... DATE: .....

TABLE OF CONTENTS

Page

List of Figures

Figure **Page**

CHAPTER 1

INTRODUCTION

Since this thesis study as well as the master's program is about Renewable energy, it's a good idea to start with the general context of renewable energy. We will begin with a brief description of the laboratory(IRDEP) were this work has been carried and the funding laboratory(IPVF). We also present the objective and motivation of our study.

IRDEP

IRDEP (Institute of Research and Development on Photovoltaic Energy)[1] is a joint laboratory of EDF, CNRS and Chimie-ParisTech. It is located at Chatou (78400) $Ile-de-France$, one of the EDF R&D site. Its activities go from fundamental research to industrial development. At the beginning, IRDEP worked on $Cu(In,Ga)(S,Se)_2$ (CIGS) materials, especially on the aspect of electrochemical synthesis of thin film CIGS. The goal is to develop efficient, cheap 2^{nd} generation of solar cells based on CIGS, compared to matured 1^{st} generation of crystalline silicon solar cells. IRDEP now works also on 3^{rd} generation solar cells (new concepts on high efficiency). Many efforts were done to contribute to the development of low-cost and environmental-friendly solar cells. New research topics include for example CIGS microcells and their micro-lens design, CZTS (Copper Zinc Tin Sulfide) and Perovskite materials, characterization of hot carrier solar cells etc. Four major research fields at IRDEP include `Silicon based technology`, `Chalcogenide thin-film based technology`,`High yield solar cells and new concepts` and `modeling and Advanced characterization`.

IPVF

The Ile-de-France Photovoltaic Institute (IPVF)[2] aims to become one of the world's main centers for research, innovation and training in the field of photovoltaic solar energy by bringing together internationally recognized academic research teams and leaders of the photovoltaic industry. IPVF aims to improve performance and competitiveness of photovoltaic cells and to develop new ground-breaking technologies. It has different project like project **J** on modeling which I worked with.

Introduction

I began my internship on the 14^{th} March 2016 and it lasted for 6 months period. I worked on the J-project of IPVF which deals with advanced modeling of solar cell materials. The internship topic is **Modeling spatial inhomogeneities in thin fim solar cells.** I carried out this internship at IRDEP laboratory and it was funded by Centre National de la Recherche Scientifique (CNRS) and IPVF. The group I worked with at IRDEP are working on advanced optoelectronic characterization, such as hyperspectral imagery of photoluminescence (PL) or electroluminescence (EL), time-resolved photoluminescence (TRPL) etc

[1] http://www.irdep.cnrs-bellevue.fr/index-en.html
[2] www.ipvf.fr

Objective of my internship

The main objective of my internship was to implement mathematical model to study the effects of spatial inhomogeneities on thin film solar cells. Also the aim was to analyze the effect of these inhomogeneities on the luminescence images(maps).

Research question

This thesis was intended to answer to two main questions; (1) How to apply mathematical models to characterize the transport properties of thin film solar cells? and (2) How to model these properties to predict and confirm experimental outcomes?

Methodology of the thesis

This thesis is mainly confined to Numerical and analytic methods. The modeling and numeric simulations were all carried out in MATLAB. Using both written scripts and pdetool box to solve the diffusion/ continuity equations using the Finite Element Method.

Significance of the thesis

The modeling would find application in the characterization of several PV technologies (from first to third generation of PV devices).

1.1 Renewable Energy sources

In modern world the demand for energy has increased dramatically in the past centuries and it will grow even further in the near future than ever before.The term 'renewable energy' has no official or commonly accepted definition. As an example, the Renewable Energy Working Party of the International Energy Agency defines renewable energy as 'energy that is derived from natural process that is replenished constantly'. The renewable energy sources are energy supplies that are refilled by natural processes at least as fast as we use them. For now Hydro, wind, solar and biomass are the common renewable energy sources.

1.1.1 Need for Renewable energy

The various activities (such as industrialization) which involve energy consumption that consequently leads to depletion of energy sources and degradation of environment are stretching the resources of our planet to breaking point. When it comes to the future of energy, the world needs a reality check. The economic growth and prosperity of any country or region in the world is related to the level of its consumption of energy. With the various developments, particularly with the Industrial Revolution, there has been a quantum leap towards the tremendous consumption

of energy which is supplied through fossil fuels such as gas, petroleum and coal. In modern world the demand for energy has increased dramatically in the past century and it will grow even further in the near future than ever before.

In 2012, the world relied on renewable sources for around 13.2% of its total primary energy supply. In 2013 renewables accounted for almost 22% of global electricity generation, and the IEA[3] Medium-Term Renewable Energy Report 2015 foresees that share reaching at least 26% increase in 2020.

The sun is a reliable, non- polluting and inexhaustible source of energy. Since the beginning of life on earth, the energy that was received by all living forms was radiated from the sun. It is time now when the mankind is on a standpoint to again depend and rely upon the sun as the main source of energy. Governments with vision have come to realize that generation of electrical power through non renewable sources of energy is not enough. The power of the future must be environmentally friendly as well.

[3]IEA:International Energy Agency:

CHAPTER 2

LITERATURE REVIEW

For the purpose of getting a clear idea of our research topic, this chapter is included to give a relatively brief description of the theoretical background in line with our research topic. Most of the information presented in this chapter can be found in any good solar cell or related physic textbook. We have tried to pick the most relevant parts and written in the most simplified way for a reader without a strong background on this topic. However the reader is advised to have a basic knowledge on the physics of semiconductors and(or) quantum mechanics.

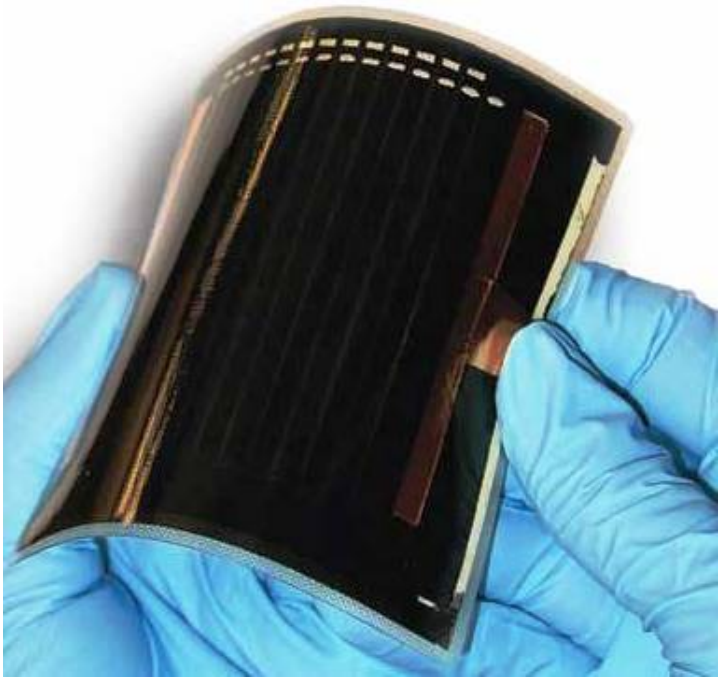

2.1 Photovoltaic Cells.

Photovoltaic (PV) cells, convert sunlight directly into electricity. PV gets its name from the process of converting light (photons) to electricity (voltage), which is called the PV effect.

2.1.1 Current outlook of PV technology

Globally the PV market is growing very fast. This calls for a simultaneous growth in the PV technology. For example: the Compound Annual Growth Rate (CAGR) of PV installations was 41% between 2000 to 2015. Concerning PV module production in 2015, China hold the lead with a share of 71%, followed by Rest of Asia-Pacific & Central Asia (ROAP/CA) with 14%. Europe contributed with a share of 5% (was 6% in 2014); USA/CAN contributed 3%.hshjsdhsfrom[10] In

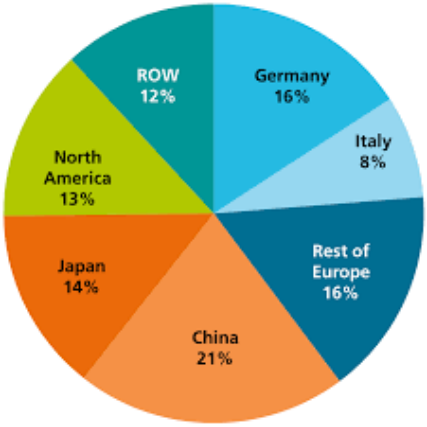

FIGURE 2.1. Cumulative PV installation by Region [10] Status 2015

2015, Europes contribution to the total cumulative PV installations amounted to 40% (compared to 48% in 2014). In contrast, installations in China accounted for 21% (compared to 17% in 2014).

Regarding the PV technology Si-wafer based PV technology accounted for about 93% of the total production in 2015. The share of multi-crystalline technology is now about 69% of total production. In 2015, the market share of all thin film technologies amounted to about 7% of the total annual production.
The record lab efficiency is 28.8% for GaAs, 25.6% for mono-crystalline silicon and 20.8%for multi-crystalline silicon wafer-based technology. The highest lab efficiency in thin film technology is 22.1% for CdTe and 22.6% for CIGS solar cells.(Since one study was mainly based on modeling thin films, in appendix A we give some general information about the thin film technology). In the last 10 years, the efficiency of average commercial wafer-based silicon modules increased from about 12% to 17% (Super-mono 21%). At the same time, CdTe module efficiency increased from 9% to 16%. In the laboratory, best performing modules are based on monocrystalline silicon with about 23% efficiency. Record efficiencies demonstrate the potential for further efficiency

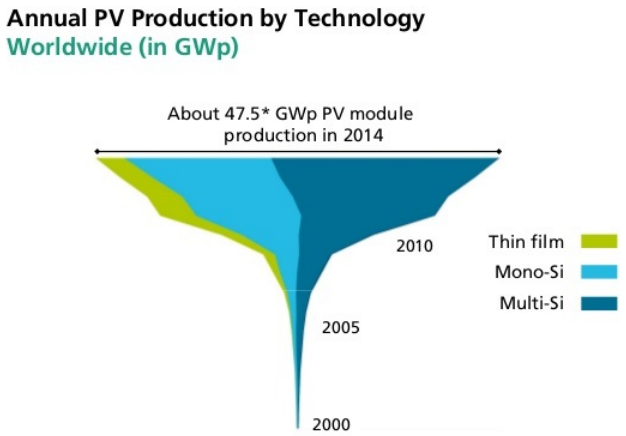

FIGURE 2.2. Cumulative PV installation by Region [14] Status 2015

increases at the production level. In the laboratory, high concentration multi-junction solar cells achieve an efficiency of up to 46.0% today. With concentrator technology, module efficiencies of up to 38.9% have been reached.

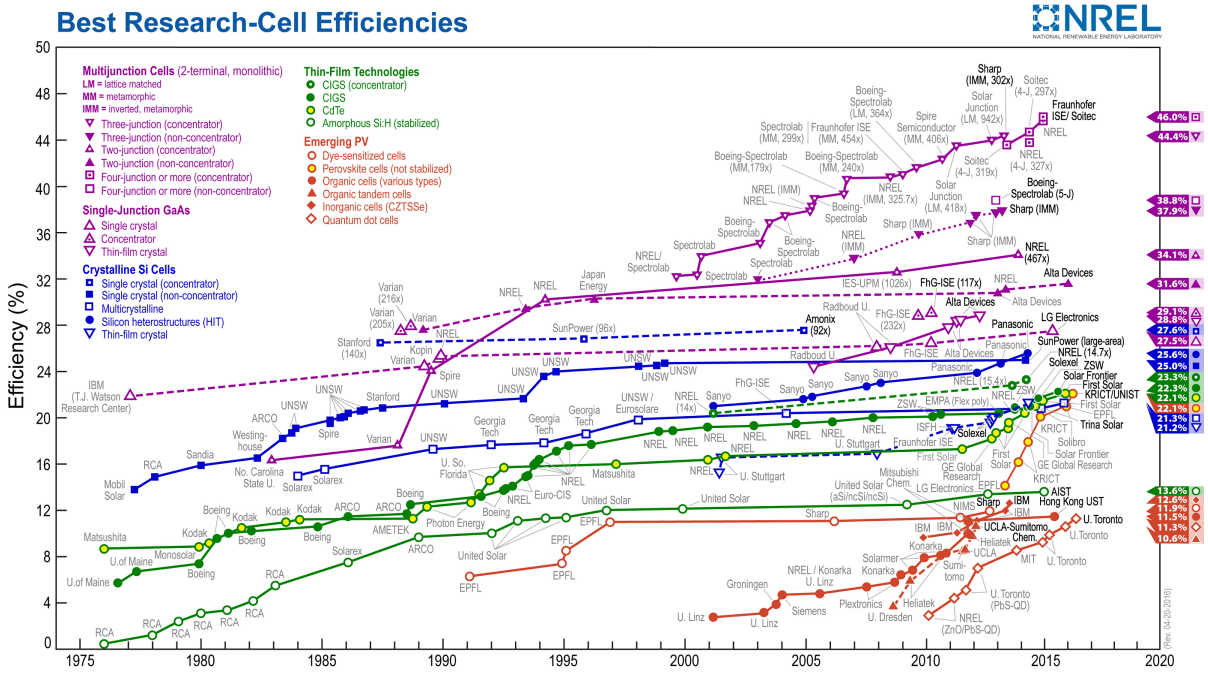

FIGURE 2.3. Research Solar Efficiecies: Chart from NREL as for 19:40, 34,April 2016 update.

2.1.2 Basic working principle of solar cell

The working principle of solar cells depends on the photovoltaic effect. Materials (mostly semiconductors) which exhibit this photovoltaic property absorb photons from light and releases charge carriers that flow through the material. There are three basic processes of the PV working principle.

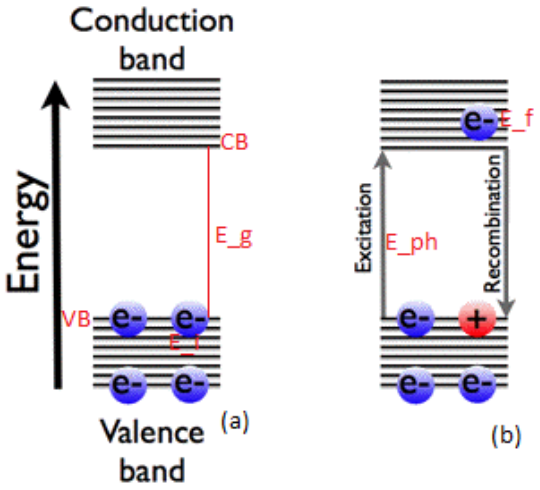

FIGURE 2.4. (a).Shows a semiconductor material in unexcited state. all the electron are in the valence band. (b).Illustrating the absorption of a photon in a semiconductor with band gap E_g. The photon with energy E_{ph} = hv excites an electron from E_i to E_f . At E_i a hole is created

1. Charge Carrier generation.(Voltage creation)
Photons with energy $E_ph \geq E_g$ might excite an electron from an initial energy level E_i to a higher energy level E_f as shown in Fig: 2.4. Photons can only be absorbed if electron energy levels E_i and E_f are present so that their difference equals to the photon energy, hv = $E_f - E_i$. In an ideal semiconductor electrons can populate energy levels below the so-called valence band edge, EV, and above the so-called conduction band edge, EC. Between those two bands no allowed energy states exist, which could be populated by electrons. Hence, this energy difference is called the band gap, $E_g = EC - EV$. If a photon with an energy smaller than Eg reaches an ideal semiconductor, it will not be absorbed but will traverse the material without interaction. If an electron is excited from E_i to E_f , a void is created at E_i. This void behaves like a particle with a positive elementary charge and is called a hole. The absorption of a photon therefore leads to the creation of an electron-hole pair.The carrier population density is governed by the the energy levels called **quasi fermi level** ε_{Fn}, ε_{Fp}. Both give the internal voltage qV = $\varepsilon_{Fn} - \varepsilon_{Fp}$

2. Separation of the photo-generated charge carriers by a PN junction.(Current Creation) After the absorption of a photon and creation of of the so-called electron hole pairs, the

electrons in the p-type materials and the holes in the n-type materials will not exist forever. They (electron and holes) will only survive for a short time range equivalent to the **minority carrier lifetime** before they recombine.On recombination, energy will then be released either as photon (radiative recombination) or transferred to other electrons or holes or lattice vibrations (nonradiative recombination). If the charge carriers recombine the energy stored in the electron-hole pairs is lost and no current or power can be generated.
If one wants to collect and use this energy, one can to use a p-n junction to spatially separate the electron and the hole. The carriers are separated by the action of the electric field existing at the p-n junction followed by a diffusion process. For the minority carrier to reach the p-n junction, the time it requires the charge carriers to reach the junction must be shorter than their lifetime. This requirement limits the thickness of the absorber.

3. Collection of the photo-generated charge carriers at the terminals of the junction
This is the final process where the charge carriers are extracted from the solar cells with the electric contacts so they can be used to perform work in an external circuit. The electro-chemical energy of the electron/hole carriers, ε_{Fn}, ε_{Fp} is finally converted to electric energy. After the electrons passed through the circuit, they will recombine with holes at a metal absorber interface.

It is very important before we finish with the solar cell operation also to mention the **loss mechanisms** involved in the cell's operation. There are two major loss mechanisms involved in single band solar cells: (1). the inability to convert photons with energies below the bandgap to electricity and (2). thermalisation of photon energies exceeding the bandgap. Thus,the maximal energy conversion efficiency of a single junction solar cell is considerably below the thermodynamic limit. This single bandgap limit was first calculated by Shockley and Queisser in 1961[15].

2.2 Carriers Transport Phenomena

The generation of electron from the valence band to the conduction band by an energetically incident photon, leads to the creation of an electron-hole pair. Electrons in the conduction band and holes in the valence band have to move in the different directions to produce an electrical charge current j_Q. The motion of an electron in a crystal is similar to the motion of a molecule in a gas. It executes a free path between collisions moving in a perfectly random when no field is applied. Under the influence of a field a drift motion is set up. The length of actual path described by the electron is much greater than the distance it has drifted under the field, and its actual velocity of motion much greater than the drift velocity[1]. The velocity of the carriers is determined by the temperature of the lattice. The thermal velocity is an average carrier velocity. Carriers have a thermal velocity that is normally distributed around this average thermal velocity. Therefore,

[1]The drift velocity is the flow velocity that a particle, such as an electron, attains in a material due to an electric field. It can also be referred to as axial drift velocity.

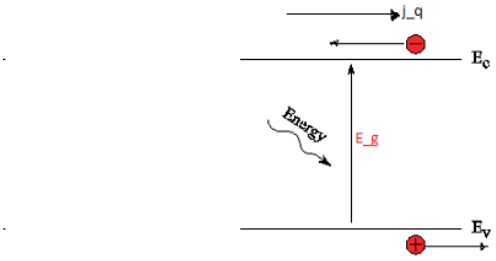

FIGURE 2.5. Shows Electron in the conduction band and hole in the valence bands move in different direction. Shows also the direction of the electrical charge current J_q.

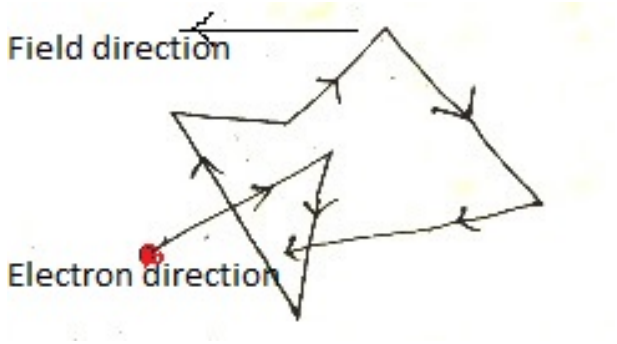

FIGURE 2.6. Path of an electron in a crystal under the influence of the electric field

some carriers having a greater velocity and some lower. Each direction of carrier movement is equally likely, therefore the motion of a carrier in one direction will eventually be balanced by the movement of the carrier in the opposite direction.

2.2.1 Drift current

We already mentioned that in the absence of an electric field, carriers move a certain distance at a constant velocity in a random direction. However, in the presence of an electric field, superimposed on this random direction, and in the presence of thermal velocity, carriers move in a net direction. There is an acceleration in the direction of the electric field if the carrier is a hole or opposite to the electric field if the carrier is an electron. The acceleration in a given direction causes a net motion of carriers over a certain net distance. Transport of carriers due to the presence of an electric field is called **drift transport**. In one dimension, the drift current for both electron and holes is expressed as:

$$J_n = qn\mu_n E_y \tag{2.1}$$

and

$$J_p = qp\mu_p E_y \tag{2.2}$$

were J_y is the drift current in y direction, E_y - applied electric field in y direction, q- electron charge n and p are the electron and hole concentrations, μ_n and μ_p electron and hole mobility.

2.2.2 Diffusion Current

The incident photon on the solar cells, generates carriers at the cell's surface but not in the bulk of the solar cell. This results in a carrier concentration gradient with the semiconductor material. When a carrier concentration gradient exists in the semiconductor, through random motion, carriers will have a net movement from areas of high carrier concentration to areas of low concentration in the process of **diffusion.** The rate at which diffusion occurs depends on the velocity at which carriers move and on the distance between scattering events. It is termed **diffusivity** and measured in $cm^2 s^{-1}$. With time, these carriers will diffuse throughout the cell until the concentration is uniform. In one dimension the diffusion current for both electron and holes is given as;

$$J_{ndiff} = qD_n \frac{\partial n(y)}{\partial y} \tag{2.3}$$

and

$$J_{pdiff} = qD_p \frac{\partial p(y)}{\partial y} \tag{2.4}$$

where
J_n and J_p is electron and hole diffusion current, q - electron charge,
D_{ndiff} and D_{pdiff} -Diffusion coefficients for electrons and holes,
n and p - electron and hole concentrations.

2.2.3 Diffusion Length of Minority Carriers

For the successful conversion of electro-chemical energy into electrical energy, our aim is to make sure that the charge carriers produced by the absorption of a photons, as many as possible flow toward the terminals of the solar cell. However this is not an obvious case, the existence of the driving force for the charge carriers is not sufficient. Since the electrons and holes recombine after a lifetime, they must also be able to reach the terminals in this time frame. For example to see how far an electron can travel by diffusion before it vanishes by recombination, lets take a case where electrons are injected with a current density j_n into a p- conductor as minority charge carriers (see figure 2.7) The electrons move in the x,y and z-directions, we assume a homogeneous

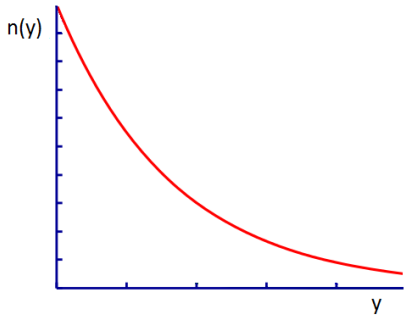

FIGURE 2.7. Distribution of electrons injected as minority charge carriers into p-conductor

system. The steady state distribution of the additionally injected electrons in the y-direction is given by the **continuity equation** [22].

$$\frac{\partial n_n}{\partial t} = G_n - R_n - divJ_n = 0 \tag{2.5}$$

were n_n is the electron concentration density, G_n - electron generation term and R_n - Recombination term.
For the particle diffusion current;
$j = -D_n \frac{\partial n}{\partial y}$ hence div$j = -D_n \frac{\partial^2 n}{\partial y^2}$
In the p-conductor,

$$G = G^0 = \frac{n^0}{\tau_n}$$

and

$$R = \frac{n(y)}{\tau} = \frac{n^0}{\tau} + \frac{\Delta n(y)}{\tau}$$

It then follows from equation 2.5 that

$$-\frac{\Delta n(y)}{\tau} + D_n \frac{\partial^2 \Delta n(y)}{\partial y^2} = 0 \tag{2.6}$$

The solution for this differential equation takes the form;

$$\Delta n(y) = \Delta(0) \exp(-\frac{y}{L_n}) \tag{2.7}$$

The characteristic length L_n is the diffusion length which in our case is for the electron. Substituting this result into Equation 2.7 we obtain

$$L_n = \sqrt{D_n \tau_n} \tag{2.8}$$

The **diffusion length** is the mean path length for the diffusion of a charge carrier during its lifetime. One should note that in a homogeneously illuminated pn structure, only those electrons

that are generated in the p-conductor at a distance not larger than their diffusion length will reach the n- conductor. Once the electrons are within the n-conductor, in a region in which the electrons are the majority charge carriers, their recombination has no effect on the charge current. Even though they recombine in the n-conductor, recombination does not eliminate their charge. Since the charge is transported by the majority carriers, other electrons continue to transport the charge. Recombination here reduces the charge current only if it affects the minority carriers produced by the illumination[22].

2.3 Recombination of Electrons and Holes

The electron-pairs created by the absorption of an energetic photon, will not stay forever in the material but instead it will recombine after a very short time (lifetime). Recombination is associated with the lifetime of the material, and thus of the solar cell. There are three basic categories of recombination: (a) direct recombination, (b) recombination through traps, (c) surface recombination.

In **direct recombination**, the electrons and holes combine through an electron dropping from a state in the conduction band to an empty state in the valence band in a single transition. An amount of energy ΔE is converted into radiation. The radiation may or may not also involve the emission of absorption of phonons. In most books direct recombination is also reffered to as radiative recombination.

Recombination through traps also called Shockley-Read-Hall or SRH recombination, the recombination of electrons and holes does not occur directly from bandgap to bandgap. It is facilitated by a impurity atom or lattice defects. Their concentration is usually small compared to the acceptor or donor concentrations.These recombination centres introduce allowed energy levels within the forbidden gap, so-called **trap states.** An electron can be trapped at such a defect and consequently recombines with a hole that is attracted by the trapped electron. Though this process seems to be less likely than the direct thermal recombination, it is the dominant recombination-generation process in semiconductors at most operational conditions . The process is typically non-radiative and the excess energy is dissipated into the lattice in form of heat. The name is a reverence to William Shockley, William T. Read and Robert N. Hall, who published the theory of this recombination mechanism in 1952 [16]. Other related to SRH recombination but not similar is the so-called Auger Recombination.

Auger Recombination involves three carriers. An electron and a hole recombine, but rather than emitting the energy as heat or as a photon, the energy is given to a third carrier, an electron in the conduction band. This electron then thermalizes back down to the conduction band edge.

Auger recombination is most important at high carrier concentrations caused by heavy doping or high level injection under concentrated sunlight. In silicon-based solar cells (the most popular), Auger recombination limits the lifetime and ultimate efficiency. The more heavily doped the material is, the shorter the Auger recombination lifetime.
It was not in the scope of this work to describe the recombination mechanisms in details. We just gave a rather general idea of how these recombination processes occurs. However since part of our model will study the effect of surface recombination, we therefore saw that it was important to describe in a relatively simple details about surface recombination. For the other recombination categories mentioned and not mentioned above, the reader is advised to find more details in references [18] and [6].

2.3.1 Surface Recombination

All the recombination mechanisms described above takes place the bulk of a single-crystal semiconductor. However in some cases electrons and holes may diffuse to the surface and recombine there. Under some conditions, the rate of recombination at the surface may even be much greater than the bulk recombination rate. Therefore for many technological applications, cautions must be taken to reduce the effect of surface recombination especially at the contacts. For example in thim-film technology if the surface recombination is not treated well, it may dominate the decay process and negate the advantages of a long bulk lifetime.

In equilibrium, the number of electrons flowing to the surface of a p-tyoe crystal must be equal to the number of electrons flowing from it. The later include electrons reflected and electrons emitted. When equilibrium is disturbed these will no longer be equal. Forsmall deviation from equilirium, we expect the number emitted to be independent of the deviation. If r is the probability of reflection of an electron striking the surface, then the rate at which electrons flow to the surface is equal to $\frac{1}{4}v_t n$ for unit area, where v_t is the average thermal velocity. The rate at which electrons flow from the surface is $\frac{1}{4}v_t n + S$, S here is the rate of emission per unit area.
In equilibrium we have;

$$\frac{1}{4}v_t n_0 = \frac{1}{4}r v_t n_0 + S_0 \tag{2.9}$$

$$S_0 = \frac{1}{4}(1-r)v_t n_0 \tag{2.10}$$

The net rate S_a at which holes are absorbed by the surface is then given by

$$S_a = \frac{1}{4}(1-r)v_t(n-n_0) \tag{2.11}$$

which can be written as

$$S_a = s\Delta n \tag{2.12}$$

Effect of surface recombination to equilibrium recovery. At a distance from the surface greater than a diffusion length, the effect will clearly be small. If for example we consider a plane surface, and let x be the distance of a point in the semiconductor from the surface. We suppose a uniform generation of excess of carriers throughout the bulk of the material at a rate G; we then have to solve the continuity equation of the form

$$D_n d^2 \frac{\partial \Delta n}{\partial y^2} - \frac{\Delta n}{\tau} + G(y) = 0 \tag{2.13}$$

The surface recombination enters into the problem as a boundary condion at y = 0[18]; here we have

$$D_n \frac{\partial \Delta n}{\partial y} = s\Delta n(y = 0) \tag{2.14}$$

where -D_n is the diffusion cofficient for electron and s - recombination velocity.

2.4 Characterization techniques

In recent years, a wide and continuously increasing variety of sophisticated and rather specialized analysis techniques originating from very different directions of physics, chemistry, or materials science has been applied in order to extend the scientific base of thin-film photovoltaics. The choice of characterization techniques is not intended for completeness but should be a representative cross section through the scientific methods that have a high level of visibility in the recent scientific literature. Electrical device characterization, electroluminescence, photoluminescence,and capacitance spectroscopy are standard optoelectronic analysis techniques for solid-state materials and devices but are also well established and of common use in their specific photovoltaic context. In contrast, characterization of light trapping is an emerging research topic very specific to the photovoltaic field.

The disordered nature of most especially thin-film photovoltaic materials requires analysis of electronic, structural, and compositional properties at the nanometer scale. This is why methods such as scanning probe techniques as well as electron microscopy and its related techniques gain increasing importance in the field. X-ray and neutron diffraction as well as Raman spectroscopy contribute to the analysis of structural properties of photovoltaic materials. Since thin-film solar cells consist of layer stacks with interfaces and surfaces, important issues are addressed by understanding their chemical and electronic properties, which may be studied by means of soft X-ray and electron spectroscopy.
Combining experimental results from materials analysis with those from ab-initio calculations and numerical simulation provides the means to study point defects in photovoltaic materials. By means of carefully designed optical and electronic simulations,photovoltaic performances of specific devices may be studied even before their manufacture.

Discusion of Thin-film characterization methods, is a full book on its own. Therefore to fit the scope of our work we decided to rather limit ourselves to Luminescence characterization technique because is in line with our internship objectives. Also since the H project at IPVF is working on luminescence characterization, as we shall see in subsection 2.4.1.1 and from equastion 2.16 they are able to experimentally get the absolute value of carrier density. However for more details about all characterization techniques we suggest you read the following reference books [2], [5] and [11].

2.4.1 Luminescence characterization methods

During a solid's transition from a thermal disequilibrium to an equilibrium state, it tends to emit light. That's when luminescence reveals itself as a powerful tool towards describing this emission of light. Later on, the type of luminescence will be defined according to the excitation source we tend to use, which actually brought the system out of its thermal equilibrium. So, in case of an external voltage applied as the excitation source, then we speak of electroluminescence (EL), and for our case, we are mainly interested by the photoluminescence (PL), which corresponds to absorption of light of sufficient energy. Therefore, the source of PL radiation is the transition of electrons from higher occupied electronic states into lower unoccupied states where it recombines with a hole, under the emission of a photon. It is actually these emitted photons that will represent our PL signal, which we analyze in order to reveal crucial information about the performance of our thin film solar cell.
Comparing to other investigation techniques, PL imaging is non-destructive, non-invasive, and can actually be performed for each fabrication step of our solar cells. We must note that there are other types of luminescence such as: Cathodoluminescence, thermoluminescence, etc.

2.4.1.1 Physical phenomena of Photoluminescence

In section 2.3 we discussed different recombination mechanisms, though we didn't go in deep details and the mathematical expression about the recombination processes. We must distinguish between radiative lifetime τ_{rad} related to PL and non radiative lifetime τ_{nonrad} related to both Auger and SRH processes. For the material itself, the total recombination lifetime will include the two previous lifetimes such as

$$\frac{1}{\tau_{tot}} = \frac{1}{\tau_{rad}} + \frac{1}{\tau_{nonrad}} \tag{2.15}$$

While investigating our PL signals[22], we are strictly interested by τ_{rad}. But, keeping in mind that the lifetime of each recombination process depends on the intrinsic characteristics of the materials, we should than notice that SRH recombination is predominant comparing to the other two processes, since it directly depends on the defects within the material that are highly probable to exist. Although dominated by other recombination types, radiative recombinations are inevitable and always take place. From equation 2.15, we can conclude that the total τ_{tot}

is limited to significantly smaller values than τ_{rad} due to the dominance of τ_{nonrad}. For a good solar cell performance, it is crucial to have long carrier lifetimes, which will allow us to collect the photogenerated electron-hole pairs before they get involved in any recombination process. Therefore, the intrinsic material defects significantly lowering τ_{tot} are considered as performance-limiting parameters that we need to reduce.
We remind that our PL signal is based on radiative transitions, and so far we have been concerned with those taking place within the sample. However, experimentally, a measured PL signal is that emerging from our sample. Therefore, the determination of the photon flux emitted outside the solar cell has to be accomplished. But, doing so in a straightforward way requires knowledge of multiple parameters such as the absorption profile, diffusion, drift and recombination of carriers within the sample and many others, which is quite challenging. That's when we refer to assumptions in order to simplify the problem: First we assume homogeneous material properties, and that the light is emitted from the sample's surface. Finally, the photo current density detected outside the sample can be expressed by;

$$J_n = \frac{1}{4\pi^2\hbar^3c^2}\frac{a(E)E^2}{\exp(\frac{E-\Delta\mu}{K_BT})-1} \tag{2.16}$$

In equation 2.16 the absorptivity a(E) is given by a(E) = (1-R_t)(1-exp(-$a(E)d$)) with the front surface reflectivity R_t and the sample thickness d . This equation in particular is referred to as the generalized Planck's law [22]. Eventually, the illumination of our semiconductor results in the splitting in the quasi-Fermi level $\Delta\mu$ which itself leads finally to radiative recombinations that are the essence of our PL signal.

2.5 Finite Element Method (FEM)

Our differential equations used to get the numerical solutions were solved using the finite element method formulated in MATLAB. For this reason we decided in a few paragraphs to give a general idea of FEM for the readers with no idea about it. For more details about FEM one should refer to [1, 17, 19]

2.5.1 What is Finite Element Method (FEM)

The finite element method (FEM) is a numerical technique for solving problems which are described by partial differential equations or can be formulated as functional minimization. A domain of interest is represented as an assembly of finite elements. Approximating functions in finite elements are determined in terms of nodal values of a physical field which is sought. A continuous physical problem is transformed into a discretized finite element problem with unknown nodal values. For a linear problem a system of linear algebraic equations should be solved. Values inside finite elements can be recovered using nodal values.

There are two main features of FEM;
1). Piece-wise approximation of physical fields on finite elements provides good precision even with simple approximating functions (increasing the number of elements we can achieve any precision).
2). Locality of approximation leads to sparse equation systems for a discretized problem. This helps to solve problems with very large number of nodal unknowns.

2.5.2 How FEM works

The steps list below gives a summary of how the FEM solution works.
1). **Discretize the continuum** The first step is to divide a solution region into finite elements. The finite element mesh is typically generated by a preprocessor program. The description of mesh consists of several arrays main of which are nodal coordinates and element connectivities.
2). **Select interpolation functions**. Interpolation functions are used to interpolate the field variables over the element. Often, polynomials are selected as interpolation functions. The degree of the polynomial depends on the number of nodes assigned to the element.
3. **Find the element properties** The matrix equation for the finite element should be established which relates the nodal values of the unknown function to other parameters. For this task different approaches can be used; the most convenient are: the variational approach and the Galerkin method.
4. **Assemble the element equations** To find the global equation system for the whole solution region we must assemble all the element equations. In other words we must combine local element equations for all elements used for discretization. Element connectivities are used for the assembly process. Before solution, boundary conditions (which are not accounted in element equations) should be imposed.
5. **Solve the global equation system** The finite element global equation system is typically sparse, symmetric and positive definite. Direct and iterative methods can be used for solution. The nodal values of the sought function are produced as a result of the solution.
6. **Compute additional results** In many cases we need to calculate additional parameters. For example, in mechanical problems strains and stresses are of interest in addition to displacements, which are obtained after solution of the global equation system.

CHAPTER 3

MODELING,RESULTS AND DISCUSSION

Having introduced the main concept of our work, in this chapter we present the models used in order to achieve the objectives of our study. Here we show how we modeled the effect of lifetime, boundary condition, grain boundaries, lateral diffusion and global illumination both in 1D and 2D case. In order to simplify our work and allow the reader to follow, in this chapter we combined both modeling and the respective results.

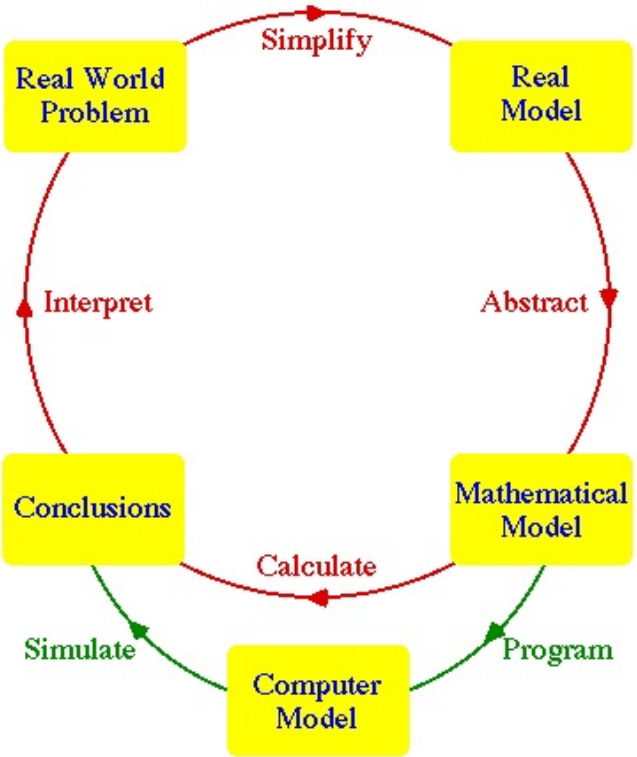

Description of the Model

Modeling the luminescence spectrum or mapping highly depend on the physical properties of a material. The spatial diffusion of photo carriers depend on the lifetime and diffusion length of the studied material. Local or global excitation can be carried out during luminescence experiments on either mono-crystalline or poly-crystalline samples.
In our study we are considering four cases (see figure 3), **case 1** we consider a homogeneous material and the excitation is uniform/global allover the sample. **Case 2**, we modeled a homogeneous material with local excitation in order to study the diffusion of carriers within the sample, related work has been done by Paget et al [3], where he was determining ambipolar diffusion on GaAs. In **case 3** and **case 4** we modeled inhomogeneous material with global and local excitation respectively, this is related to the work by P. Gundel et al [9] done on silicon to experimentally probe the effect of grain boundaries on luminescence imaging. We carried out our simulations in both 1D and 2D case, our numerical solutions have been validated with the respective analytic solutions.

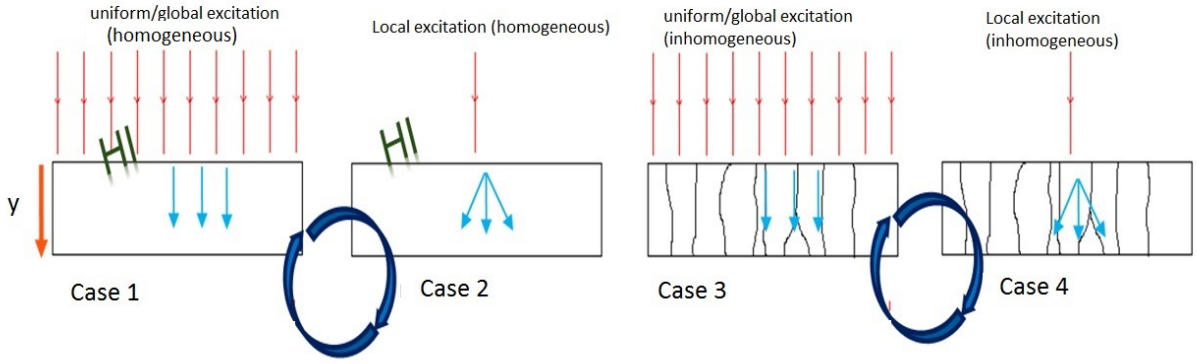

FIGURE 3.1. Shows the four excitation modes used in our model

3.1 Case 1

3.1.1 Uniform/global excitation: Homogeneous material

To really understand and validate our model, we started with the simple case of 1D problem. First, we assumed a homogeneous system with infinite boundary conditions. From the diffusion equation one can quantitatively show the relation between minority-carrier concentration and

diffusion length.

$$D\nabla^2 n(y) - \frac{n(y)}{\tau} + G_0(y) = 0 \tag{3.1}$$

where,
n(y) - is the carrier concentration along distance y,
G(y) - minority carrier injection/generation rate,
τ - minority carrier lifetime (Recombination term), and
D - the Diffusion coefficient.
In our model as from equation 3.1, we assumed a system with no Electric field (bulk absorber) and thus the only transport mechanism is diffusion.

Model

We considered a homogeneous system with uniform/global excitation. The injection rate G = $10^{18}\text{cm}^{-3}s^{-1}$, the lifetime τ = 10^{-8}s and diffusion coefficient D = 0.32375. We did not include recombination velocity therefore we assumed infinity boundary conditions.

(a)

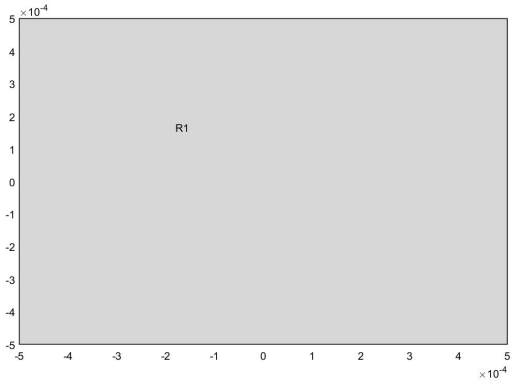

FIGURE 3.2. (a) Shows model with uniform excitation in all the region R_1.

Results and discussion

The results show uniform carrier map and profile along distance y (see figure 3.3). However we see that the density of carriers collected has decreased from 10^{18}cm^{-3} to 10^{10}cm^{-3}. This result indicates the effect of recombination, which means that when carriers are injected into the material, part of them will recombine, depending on the transport properties of the material.This result shows similar behavior as the work done by Gundel at al. ref [9]. When one carry out a luminescence experiment the values of G is known and Δn is the excess carrier density collected,

(a)

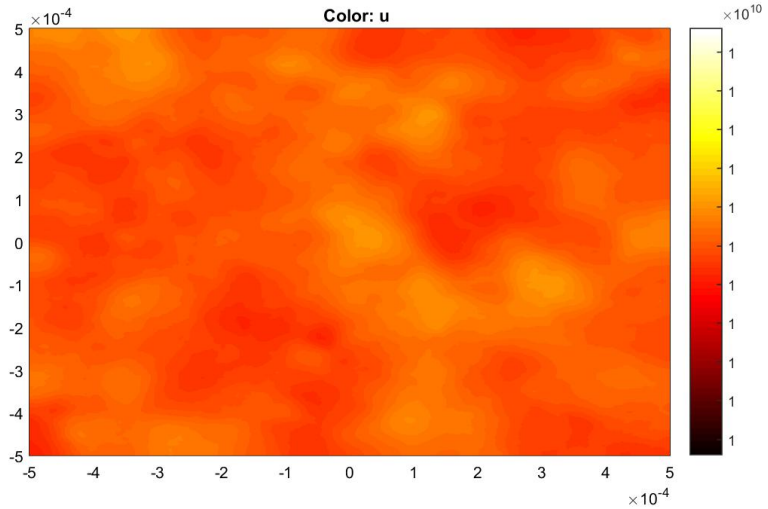

(b)

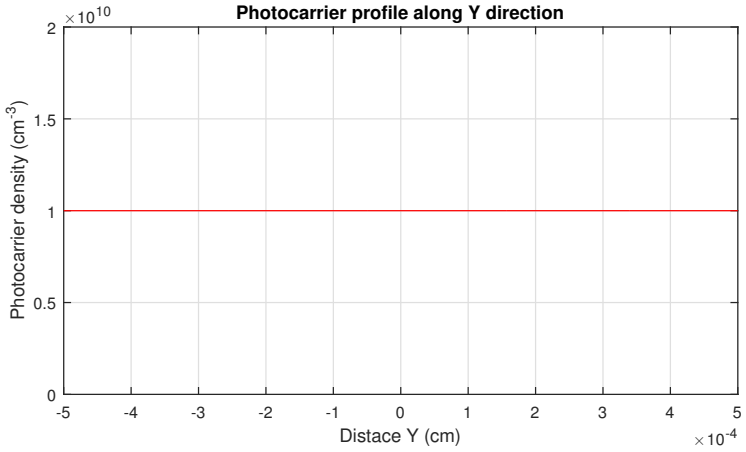

FIGURE 3.3. (a) 1D Carrier map. (b) Carrier profile along distance (y)

therefore we can use this results to compute the carrier lifetime using the simple relation $\tau = \frac{\Delta n}{G}$ as done by Trupke et al. ref [20]. For example if we insert the values of G and Δn (from figure3.3(b)), we are able to get the lifetime value($\tau = 10^{-8}$s) used in our simulation.

3.2 Case 2

3.2.1 Local excitation: Homogeneous material

We also started with modeling one dimension. We still solve the continuity/diffusion equation 3.1. We carried out the simulations both with and without the surface recombination velocity (s_n) taken at the edges of the whole cell.

Model

The sketch below illustrates a 1D model with three different regions R_1, R_2 and R_3. Where y_0, y_1, y_2 and y_3 are the edges of the regions, in our model we can set the boundary conditions only on edges y_0 and y_3. The excitation is only in region R_2 and it is uniform. This means that when solving the analytic solution for equation 3.1, the excitation/generation term (G) is only in region R_2.

y0.
R_1
y1
y1.
R_2
y2
y2.
R_3
y3

Analytic solution with infinity BC

The solution to equation 3.1 in regions R_1, R_2 and R_3 taking infinity boundary conditions are 3.2,3.3 and 3.4 respectively.

$$n(y) = A_1 \exp(\frac{y}{L_n}) \tag{3.2}$$

$$n(y) = B_1 \exp(\frac{y}{L_n}) + B_2 \exp(\frac{-y}{L_n}) + \frac{G_0 L_n^2}{D} \tag{3.3}$$

$$n(y) = C_2 \exp(\frac{-y}{L_n}) \tag{3.4}$$

$$A_1 = B_1 - B_2 \exp(\frac{-2y_1}{L_n})$$

$$B_1 = -\frac{g_0}{2} \exp(\frac{-y_2}{L_n})$$

$$B_2 = -\frac{g_0}{2}\exp(\frac{-y_1}{L_n})$$

$$C_2 = B_2 - B_1\exp(\frac{-2y_2}{L_n})$$

where, $g_0 = \frac{G_0 L_n^2}{D}$, L_n is the diffusion length ($L_n = \sqrt{D\tau}$) and D is the diffusion coefficient. One should refer to appendix B for a detailed derivation of the solutions. **Note**,the equations 3.2, 3.3 and 3.4 are solutions in 1D and they can only be used to fit 1D numeric solution. But since its our main objective to study the spatial properties, we have to find the best expression that can be used to fit the 2D numeric solution and experimental data since experimentally we deal with local excitation and hence a 2D diffusion.To do this we have to transform equation 3.1 into polar coordinate system as;

$$\frac{1}{r}\frac{\partial(Dr\frac{\partial n(r)}{\partial r})}{\partial r} + \frac{1}{r^2}\frac{\partial(D\frac{\partial n(r)}{\partial \theta})}{\partial \theta} - \frac{n(r)}{\tau} + G_0(r) = 0 \tag{3.5}$$

The only feasible behavior of equation 3.5 is,

$$n(r) \approx C_1\exp(\frac{-r}{L_n}) \tag{3.6}$$

Were C_1 is an integration constant, r is the radial distance and L_n is minority carrier diffusion length. One should refer to appendix C for the derivation of the solution.

Analytic solution with surface recombination

To study the impact of surface recombination, using the same model above we introduced the surface recombination velocity (s_n) into our problem as a boundary condition at the edges of region A and B.

$$D_n\frac{\partial \Delta n}{\partial y} = s_n \Delta n(y = 0) \tag{3.7}$$

The 1D analytic solutions with surface recombination for regions R_1, R_2 and R_3 are given in equations 3.8, 3.9 and 3.10 respectively;

$$n(y) = A_1\exp(\frac{y_2}{L_n}) + A_2\exp(\frac{-y_2}{L_n}) \tag{3.8}$$

$$n(y) = B_1\exp(\frac{y_2}{L_n}) + B_2\exp(\frac{-y_2}{L_n}) + g_0. \tag{3.9}$$

$$n(y) = C_1\exp(\frac{y_2}{L_n}) + C_2\exp(\frac{-y_2}{L_n}) \tag{3.10}$$

with

$$A_1 = B_1 + \frac{g_0}{2}\exp(\frac{-y_1}{L_n})$$

$$A_2 = \frac{-w}{x} A_1 \exp(\frac{2y_O}{L_n})$$

$$B_1 = C_1 - \frac{g_0}{2} \exp(\frac{-y_2}{L_n})$$

$$B_2 = A_2 - \frac{g_0}{2} \exp(\frac{y_1}{L_n})$$

$$C_1 = -\frac{w}{x} C_2 \exp(\frac{-2y_3}{L_n})$$

$$C_2 = \frac{g_0}{2}\frac{wp}{x}\left(\exp(\frac{2y_0}{L_n} - \frac{y_2}{L_n}) - \exp(\frac{2y_0}{L_n} - \frac{y_1}{L_n})\right) + \frac{g_0}{2p}\left(\exp(\frac{y_2}{L_n} - \frac{y_1}{L_n})\right)$$

with, $x = \frac{SL_n}{D} + 1$ and $w = \frac{SL_n}{D} - 1$ and
$p = 1 - \frac{w^2}{x^2}\exp(-2y_3/L_n + 2y_0/L_n)$.

Results and discussion

Since different materials have different properties, here we carried out three different simulations (b), (c) and (d) with lifetime $\tau = 10^{-7}s$,$\tau = 10^{-8}s$ and $\tau = 10^{-9}s$ respectively, for both 1D figure 3.4 and 2D figure 3.5. The material is homogeneous with infinite boundary conditions. The excitation was uniform and only in region R_2, with a generation rate of G= 10^{18}cm^3, and diffusion coefficient D = 0.32375.
From the maps in figure 3.4 (1D case) and 3.5(2D case), we observe that for very short lifetime, carriers diffuse at very short distances as in figures 3.4(d) and 3.5(d) for 1D and 2D respectively. This is because from equation 3.1, the recombination term increases for shorter lifetime, which means, the generated carriers recombine very fast before reaching the surface of the material. This result is important because during some luminescence experiments one might fail to observe any signals when the recombination is too high. The diffusion length (L) is connected to the lifetime as $L = \sqrt{D\tau}$.

Figure 3.4(e) shows carrier profile for the numeric simulations in 1D fitted with the analytic solutions using equations 3.2, 3.3 and 3.4. From the results we see a very good agreement between the two solutions which implies the validity of our numeric results. However we see a small deviation of the two solutions at the boundaries, for the simulation carried out with long lifetime, this might be due to the boundary conditions approximations, set during FEM formulation of the program used to carry out our simulations.

Figure 3.5(e) shows the carrier map transformed from the 2D Cartesian coordinates system to polar coordinates system. The profile in figure 3.5(f) shows the decay of carriers along radial distance r. We used the analytic expression in equation 3.6 to fit the numerical simulation result which also shows a good agreement.
Figure 3.6 shows carrier profiles with **Surface Recombination velocities**. We see from figure

3.6(a) that as the surface recombination velocity s_n increases, the carrier profile decays to zero. This indicates the effect of increased recombination at the surface, we also observe the decrease in the peak of carrier density as a result of high surface recombination, which implies that surface properties affect the overall performance of the material. Figures 3.6(b) and 3.6(c) show profiles with analytic fits, which show a good agreement with the numeric results for both 1D and 2D respectively. Note, in our simulation we used a relatively long lifetime i.e ($\tau = 10^{-7}$s) in order to clearly observe the effect of surface recombination. Recall that the surface recombination was modeled as a boundary condition.

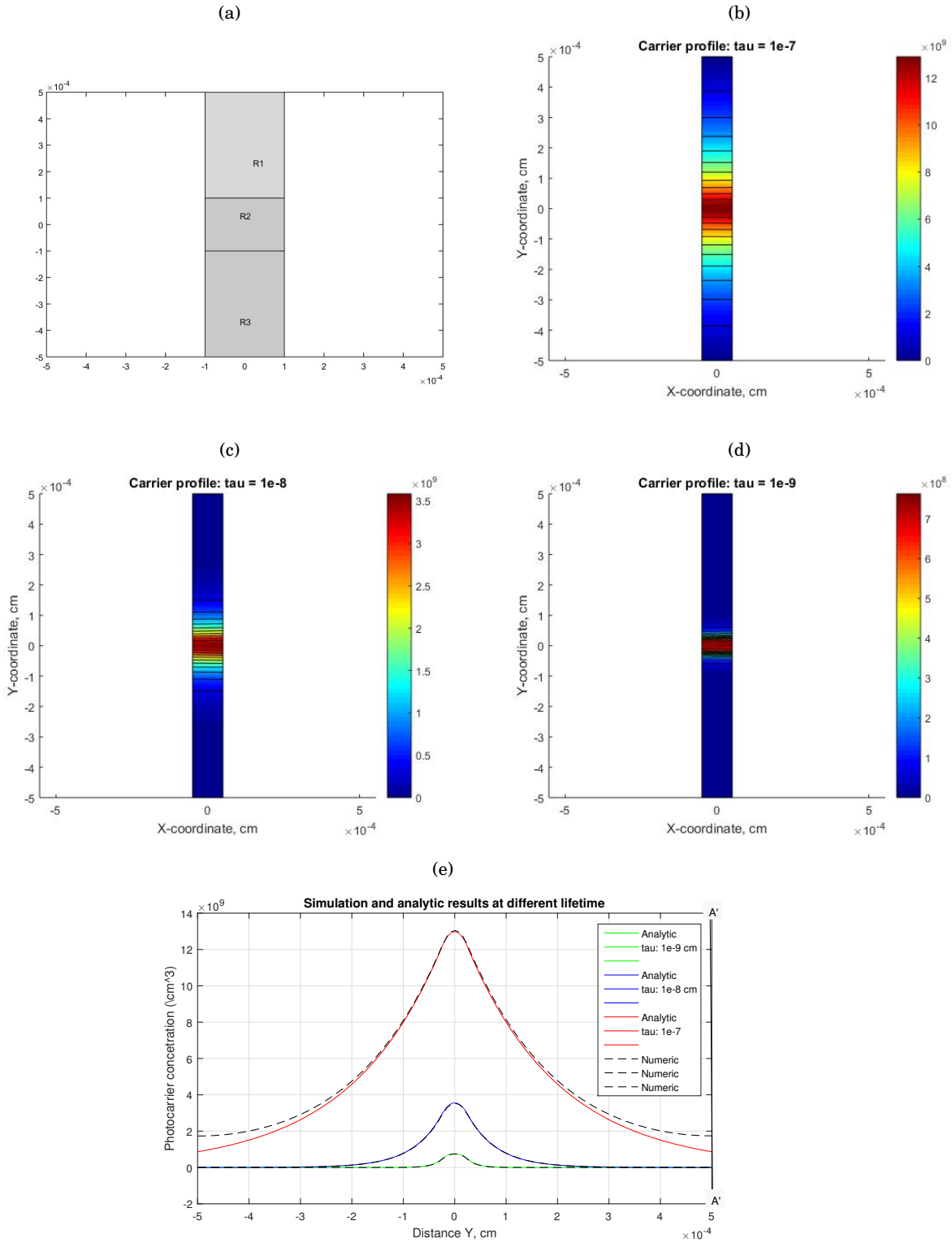

FIGURE 3.4. (a) simulation model with excitation in region R_2 only. (b) simulation with long lifetime i.e ($\tau = 10^{-7}s$). (c) Simulation with $\tau = 10^{-8}s$. (d) simulation with $\tau = 10^{-9}s$ (e) dotted line is the numeric result with corresponding analytic solution in colors i.e ($red\tau = 10^{-7}s$, blue $\tau = 10^{-8}s$ and green $\tau = 10^{-9}s$)

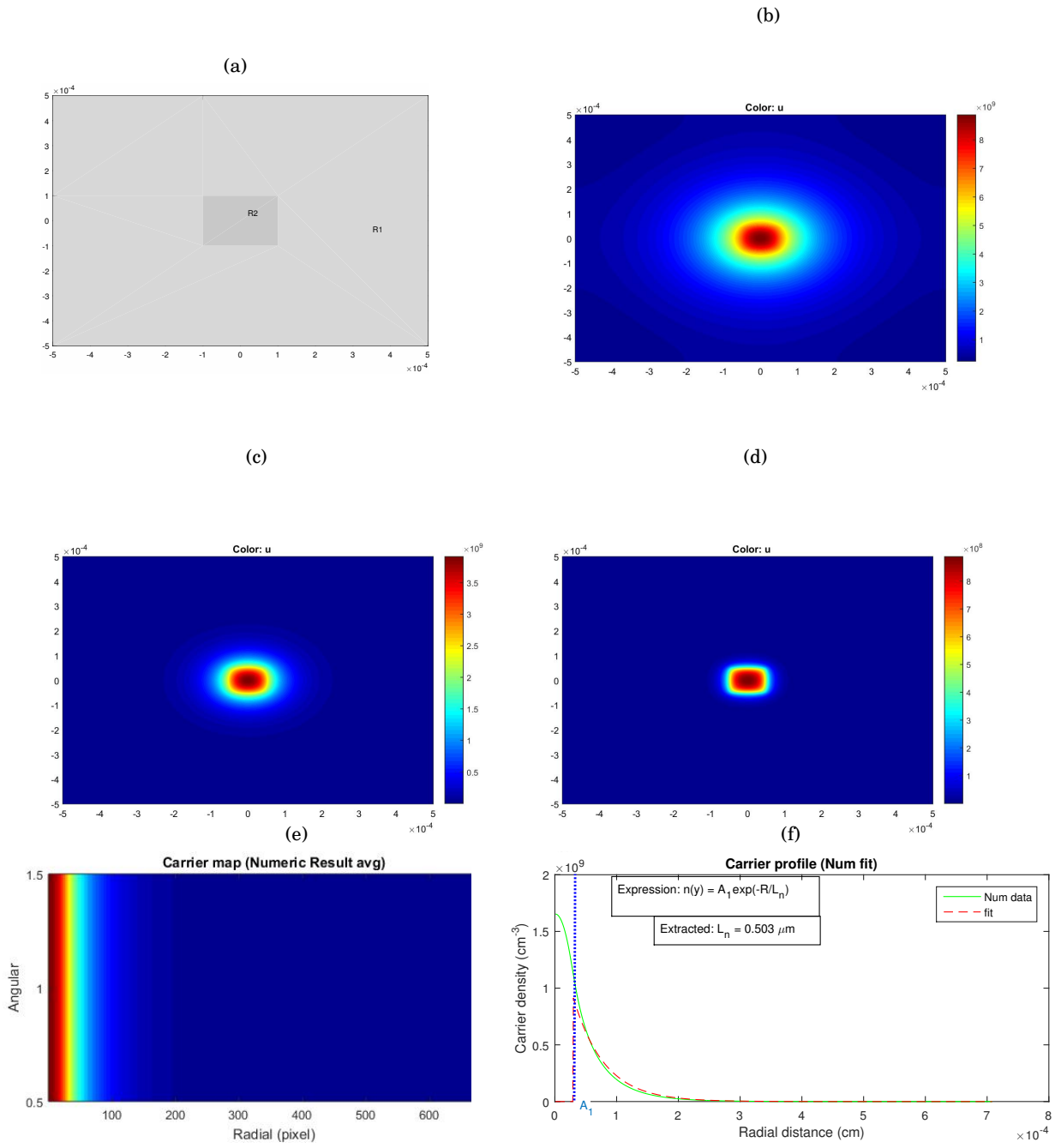

FIGURE 3.5. (a) simulation model with excitation in region R_2 only. (b) simulation with long lifetime i.e ($\tau = 10^{-7}s$). (c) Simulation with $\tau = 10^{-8}s$. (d) simulation with $\tau = 10^{-9}s$ in Cartesian coordinates. (e) Carrier map in polar coordinates system. (f) Carrier profile along radial distance r, (red is the analytic fit).

(a)

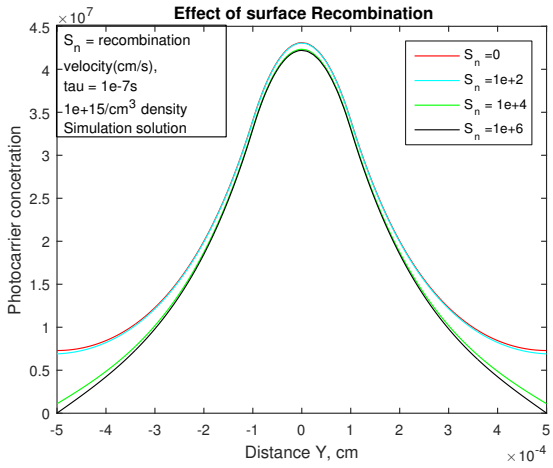

(b)

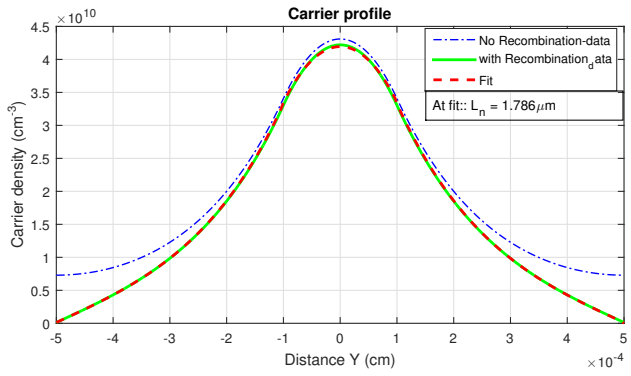

(c)

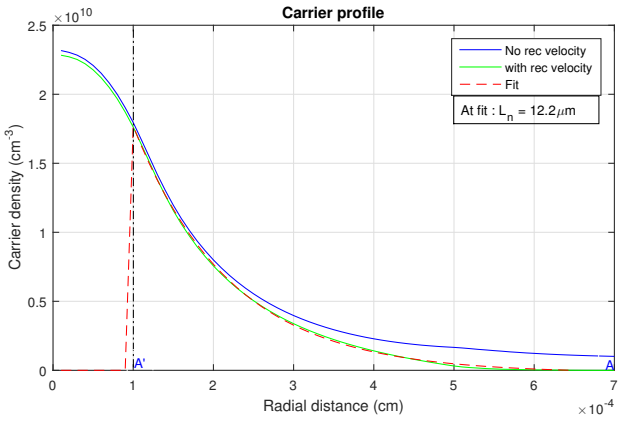

FIGURE 3.6. (a) Carrier profile along distance (y) for different recombination velocities (red =infinity BC, blue $s = 10^2$cm/s, green $s = 10^4$cm/s and black $s = 10^6$cm/s), 1D numerical results. (b) Shows analytic fit in red dotted line, green is numeric profile with a recombination of $s = 10^6$cm/s and blue is the profile with infinity boundaries for 1D. (c) 2D profile, green - numeric profile, red - analytic fit from A' to A and blue - profile with infinity boundary conditions

3.3 Case 3

3.3.1 Uniform/global excitation:Inhomogeneous material

In order to study the effect of spatial inhomogeneities, which is the main objective of our work, we modeled grain boundaries or defects by changing some transport properties in the bulk of the study material.

Model

In our model we considered an inhomogeneous system with uniform/global excitation. The injection rate is G = 10^{18}cm^3. In region R_1 the lifetime $\tau = 10^{-8}$s and $\tau = 10^{-9}$s in region R_2, the diffusion coefficient D = 0.32375. We did not include surface recombination velocity therefore we assumed infinity boundary conditions.

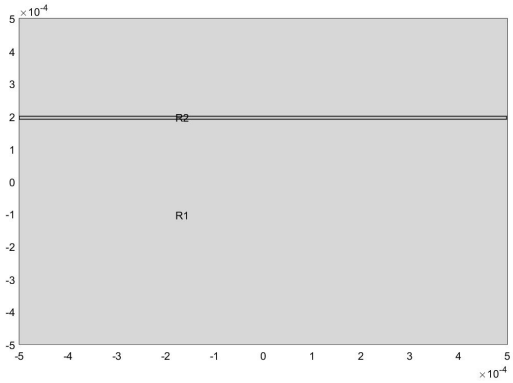

FIGURE 3.7. Shows Global uniform generation in all regions with a recombination center at region R_2

.

Results and discussion

Figure 3.8(a) shows the carrier map, we see a decrease in the intensity around the region with a shorter lifetime i.e ($\tau = 10^{-9}$s) compared to the other region with lifetime ($\tau = 10^{-8}$s). Which is a result of increased recombination rate around this region. Figure 3.8(b) shows carriers profile along distance y (cm), we see a decay in carrier concentration around the defect implying a high recombination rate. This result shows similar behavior as the work done by Gundel at al ref [9]

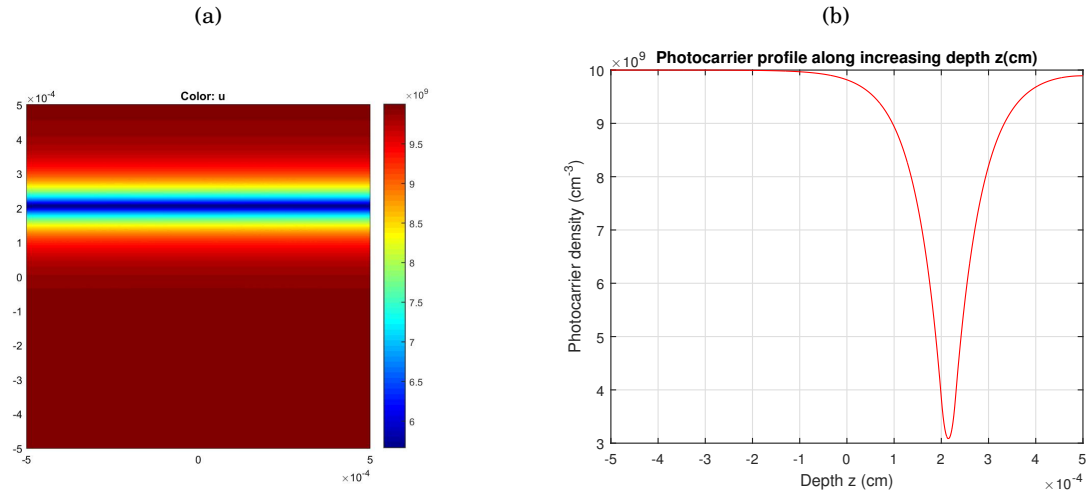

FIGURE 3.8. (a) Carrier map with grain boundary (blue region) . (b) Carrier profile along y direction.

3.4 Case 4

3.4.1 Local excitation: Inhomogeneous material

This section represent an important part of our study since it deals with modeling effect of inhomogeneties on the Lateral diffusion of carriers. We will show the effect of defect size as well as the defect lifetime property on the overall material properties. Our results will be both in 1D and 2D with there respective analytic solutions.

Model

Starting with the 1D model, the sketch below illustrates how we solved and modeled our study material. By including a region R_3 with different (shorter) lifetime (τ_2), from other regions R_1, R_2 and R_4 with a lifetime τ_1, we were able to model the effect of grains/defects in our material. From the sketch below y_0, y_1, y_2, y_3 and y_4 represent the edges of regions R_1, R_2, R_3 and R_4, Note, from the tool we used for the numeric simulations, we were only able to set the boundary conditions at the edges and not within the bulk of the material, therefore for our case on y_0 and y_4. The solutions to the continuity equation 3.1 in R_1, R_2, R_3 and R_4, with the excitation only in region R_2, and infinity BC[1] are; equations, 3.11, 3.12, 3.13 and 3.14 respectively.

[1]BC: Boundary condition

y0.
R_1
y1
y1.
R_2
y2
y2.
R_3
y3
y3.
R_4
y4

$$n(y) = A_1 \exp\left(\frac{y}{L_1}\right) \tag{3.11}$$

$$n(y) = B_1 \exp\left(\frac{y}{L_1}\right) + B_2 \exp\left(\frac{-y}{L_1}\right) + g_0. \tag{3.12}$$

$$n(y) = C_1 \exp\left(\frac{y}{L_2}\right) + C_2 \exp\left(\frac{-y}{L_2}\right) \tag{3.13}$$

$$n(y) = D_2 \exp\left(\frac{-y}{L_1}\right) \tag{3.14}$$

with,

$$A_1 = B_1 - B_2 \exp\left(\frac{-2y_1}{L_1}\right)$$

$$B_1 = C_1 \exp\left(\frac{y_2}{L_2} - \frac{y_2}{L_1}\right) + C_2 \exp\left(\frac{-y_2}{L_1} - \frac{y_2}{L_1}\right) - B_2 \exp\left(\frac{-2y_2}{L_1}\right) - g_0 \exp\left(\frac{-y2}{L_1}\right)$$

$$B_2 = -\frac{g_0}{2} \exp\left(\frac{y_1}{L_1}\right)$$

$$C_1 = C_2 \exp\left(\frac{-2y_3}{L_2}\right)\left(\frac{\frac{L_1}{L_2} - 1}{\frac{L_1}{L_2} + 1}\right)$$

$$C_2 = \Gamma(2B_2 \exp\left(\frac{-y_2}{L_1} + \frac{y_2}{L_2}\right) + g_0 \exp\left(\frac{y_2}{L_2}\right)$$

$$D_2 = C_1 \exp\left(\frac{y_3}{L_2} + \frac{y_3}{L_1}\right) + C_2 \exp\left(\frac{y_3}{L_1} - \frac{y_3}{L_2}\right)$$

were; $\Gamma = \frac{\frac{L_1}{L_2}+1}{\left(\frac{L_1}{L_2}+1\right)^2 - \left(\frac{L_1}{L_2}-1\right)^2 \exp\left(\frac{-2y_3}{L_2} + \frac{2y_2}{L_2}\right)}$.

The excitation was uniform in region R_2 only. In region R_3, the lifetime is shorter compared to regions R_1, R_2 and R_4 in both 1D and 2D model. This region with high recombination rate tends to simulate grain boundaries or a defect region. First, we carried out three simulations by changing the size of the defect/grain in order to understand the defect size impact. Then we made three other simulations, this time by changing the value of the lifetime in the defect region, in order to have an idea of what happens for different materials.

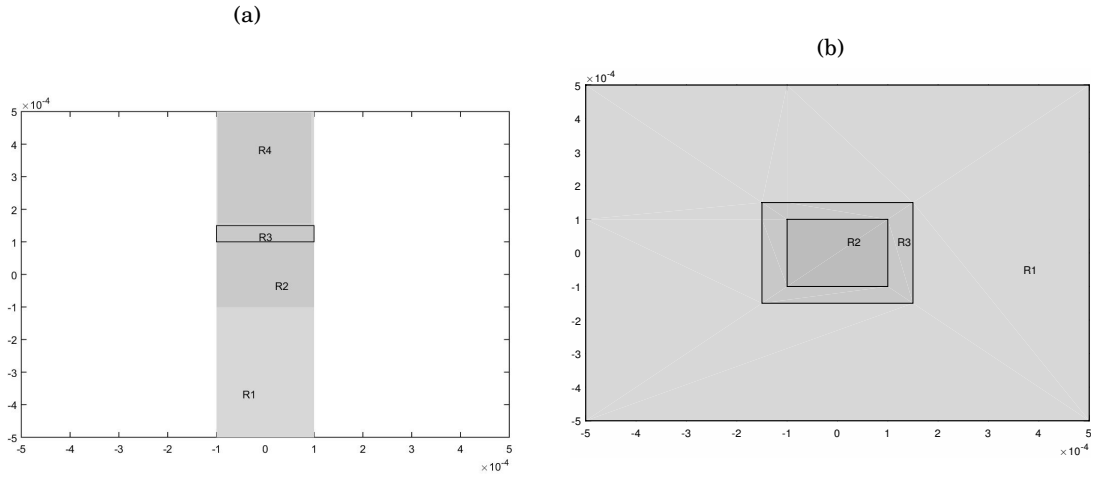

FIGURE 3.9. (a) 1D model with defect in region R_3 . (b) 2D model with defects in region R_3.

Results and discussion

From figure 3.10(b) we see that as the size of the defect increases (in blue color) the effect become more pronounce compared to the case with small grain size. This implies that however much the defect properties are more or less the same as the global materials properties, but as the size/number of the defect increase, the effect becomes more pronounced and alters the good performance of the material.

Figure 3.10(c) shows results of three simulation of lifetime in the defect region. From the carrier profile we see that the effect becomes more intense as the carrier lifetime becomes shorter (in red). Note, to clearly simulate the effect of lifetime, we made the defect size small such that we are not affected by the the size effect. This means the behavior is due to increased recombination in this region. This result implies that however small the defect size is, if the recombination is too high, it will affect the global material properties/performance.

Figure 3.11 shows the carrier maps from the simulation of defect lifetime. We see the intensity decreases as the lifetime becomes shorter, which is a result of increased recombination rate in this region. The result implies that if the recombination is too high in a particular region within the bulk of the material, we might not observe any luminescence signal during the experiment.

(a)

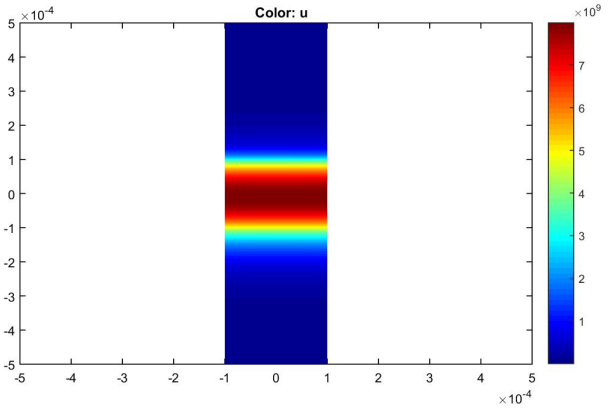

(b)

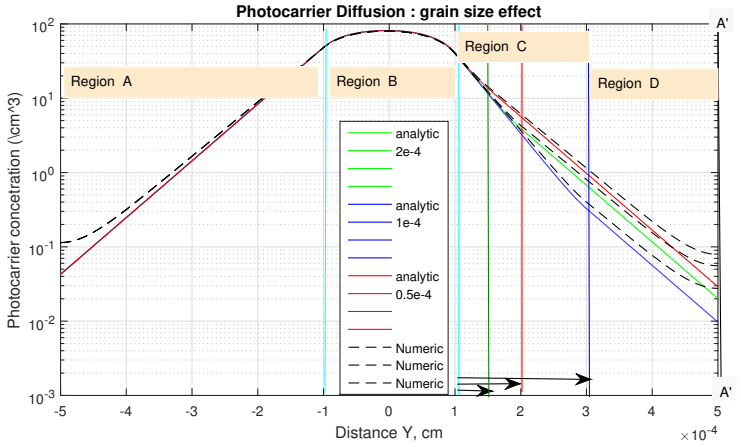

(c)

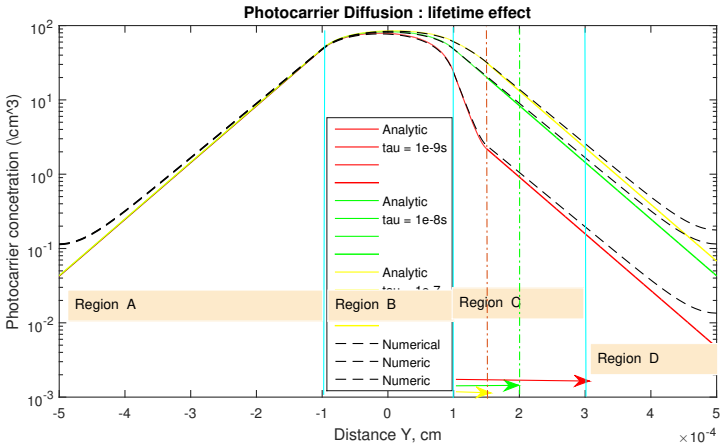

FIGURE 3.10. (a) Carrier map with grain effect at R_3i.e ($\tau = 10^{-9}s$). (b) Simulation of grain size i.e (green = $2e-4$cm, blue = $1e-1$cm and red = 5e-5cm) (c) simulation of grain lifetime i.e red$\tau = 10^{-9}s$, green $\tau = 2\times10^{-9}s$ and yellow $\tau = 6\times10^{-9}s$ here the size of $R_3 = 5e-5cm$ in all figures shows numeric(black dotted) and analytic results (in colors)

(a) (b)

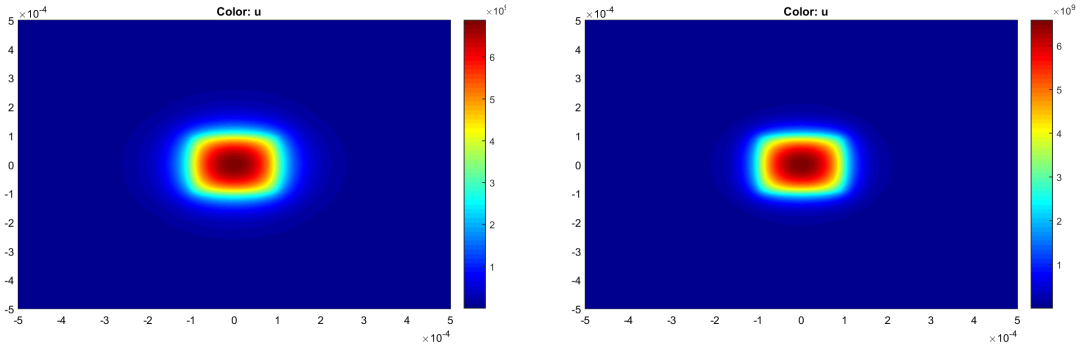

(c)

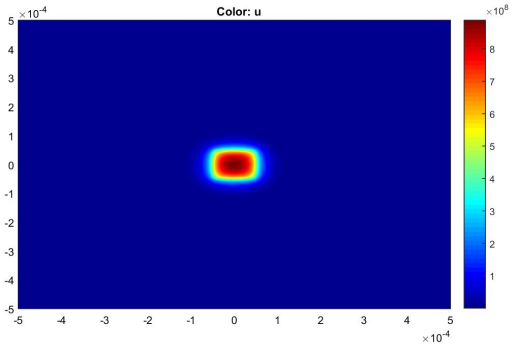

(d)

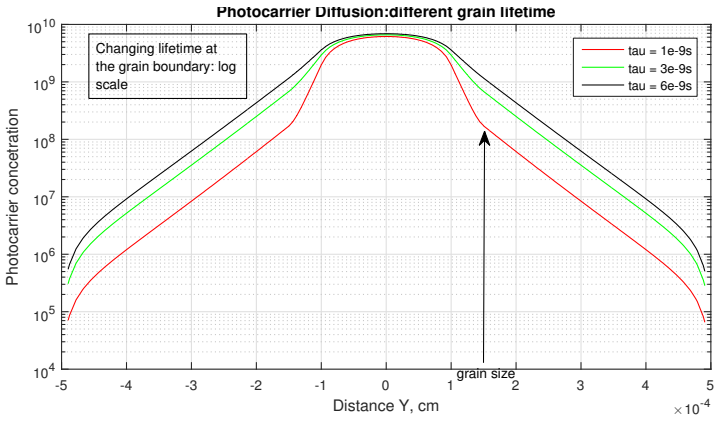

FIGURE 3.11. (a) simulation with long lifetime i.e ($\tau = 6 \times 10^{-9}s$). (b) Simulation with $\tau = 3 \times 10^{-9}s$. (c) simulation with $\tau = 10^{-9}s$, (d) Carrier profile when we make a cut along Y

CHAPTER 4

FITTING EXPERIMENT DATA

Apart from the numerical modeling, we also integrated our model to experimental domain. In the group I worked with at IRDEP, they are working on characterization of solar cells (mainly on CIGS and III-V solar cells absorber materials) using photo-luminescence imaging. But after acquiring data from the experiment, they have to find means of treating the data to extract some transport parameters like the diffusion length. They are able to determine/read the carriers lifetime, excess carrier density and other parameters directly from the experiment. However since there is not enough knowledge on the exact value of the diffusion coefficient, we cannot directly apply the simple relation $L_n = \sqrt{D\tau}$ to find the diffusion length and other required parameters. [4].

4.1 Fitting 1D numerical data

For the start, in order to have a clear idea whether the fitting procedure works well, we first fitted the data obtained in our own numerical simulations using the analytic solutions.

Homogeneous material

After carrying out the simulations in one dimension to obtain the data, we used the analytic expressions below to fit the data in different regions. These expression were used to fit the data only for a homogeneous system and with infinity boundary conditions. Since the regions have different mathematical behavior, we could not use a single expression to fit the whole profile. However we found out that one can decide to fit a single region and get the same results given that you are dealing with a homogeneous system, see section 3.2. In section 3.2, we found the analytic solutions in regions R_1, R_2 and R_3 as 4.1, 4.2 and 4.3 respectively. Recall the excitation

is local and in region R_2 only.

$$n(y) = A_1 \exp(\frac{y}{L_n}) \tag{4.1}$$

$$n(y) = B_1 \exp(\frac{y}{L_n}) + B_2 \exp(\frac{-y}{L_n}) + cst \tag{4.2}$$

$$n(y) = C_2 \exp(\frac{-y}{L_n}) \tag{4.3}$$

Inhomogeneous material

For inhomogeneous material (see section 3.3) we used the analytic solutions, equations 4.4 and 4.5 below to fit regions R_3 and R_4 (see figure 3.9(a)). Note, since the material is inhomogeneous, it implies that the transport properties are different around the defect areas. In our case the defect area was modeled as region R_3 from distance y = 0 to 3×10^{-4} cm with lifetime ($\tau_2 = 10^{-9}$s) and we used equation 4.4 to extract the diffusion length L_2. The other regions R_1, R_2 and R_4 were modeled to have the same lifetime ($\tau_1 = 10^{-8}$s). Since these regions have the same transport properties, we can fit one of them to extract the diffusion length L_1 using equation 4.5 below.

$$n(y) = C_1 \exp\left(\frac{y}{L_2}\right) + C_2 \exp\left(\frac{-y}{L_2}\right) \tag{4.4}$$

$$n(y) = D_2 \exp\left(\frac{-y}{L_1}\right) \tag{4.5}$$

Results and discussion

Figure 4.1 shows the 1D numeric data fitted with the analytic solution. In figures 4.1(a) (linear scale) and 4.1(b) (log scale) is the data from a homogeneous material with local excitation in the middle. The fitting of the three separate regions was made using the analytic solutions, equations 4.1, 4.2 and 4.3 respectively. On the fit, we were able to extract the diffusion length $L_n = 0.56\mu m$, similar to the one calculated by directly computing the diffusion length from $L_n = \sqrt{D\tau}$. where D = 0.32375 is the diffusion coefficient and $\tau = 10^{-8}$s is the carrier lifetime used in our simulations. Figure 4.1(c) shows the data fit for an inhomogeneous material. As we have already mentioned, the inhomogeneity has different transport properties, from the rest of the bulk. Using equation 4.4, we were able to fit the region from y = 0 to 3×10^{-4}cm which we modeled with life time $\tau = 10^{-9}$s. We managed to extract the diffusion length $L_2 = 0.18\mu m$ from this region and using the equation 4.5 to fit the region y = 3×10^{-4}cm to 5×10^{-4}cm, which represent the other bulk of the material with similar properties, we extracted the value of the diffusion length $L_1 = 0.51\mu m$. Both results show that we are able to extract back the same values (with accuracy error) of the diffusion length through fitting as one should get by directly computing the values used in the numeric simulations.

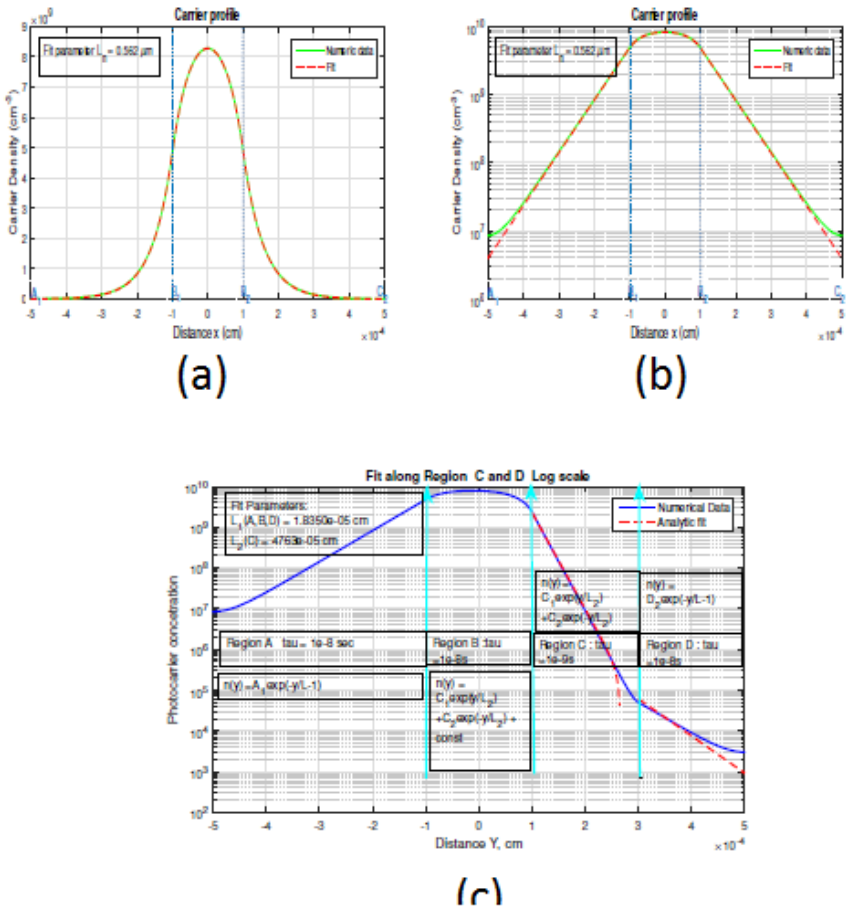

FIGURE 4.1. (a) Fit homogeneous system-linear scale. (b) Fit in log scale-homogeneous. (c) Fit for inhomogeneous material (in log scale)

Fit with surface recombination

We further carried out fitting the numerically extracted data taking into account the surface recombination. The found expressions,equations 4.6, 4.7 and 4.8, can be used to extract both the diffusion length and the surface recombination velocity s_n for 1D model (see section 3.2). In our case, the surface recombination velocity s_n was set (i.e $s_n = 10^6$cm/s) and the aim was to assess the diffusion length. In our model, the surface recombination velocity was used as a boundary condition (see appendix B.1.2). One should note that, each expression was used to fit each of the three different regions A, B, C and D of 1D model (see section 3.2) respectively.

$$n(y) = \frac{D}{s_n L_n} A_1 \exp\left(\frac{y_1}{L_n}\right) - A_2 \exp\left(\frac{-y_1}{L_n}\right) \tag{4.6}$$

$$n(y) = B_1 \exp\left(\frac{y_1}{L_n}\right) + B_2 \exp\left(\frac{-y_1}{L_n}\right) + cst \tag{4.7}$$

$$n(y) = \frac{D}{s_n L_n} C_1 \exp\left(\frac{y_3}{L_n}\right) - C_2 \exp\left(\frac{-y_3}{L_n}\right) \tag{4.8}$$

Note, in all expressions used for fitting above, R_1, R_2, R_3 and R_4 are fitting coefficients whose values are estimated from the initial fitting guess and cst stands for constant.

Results and discussion

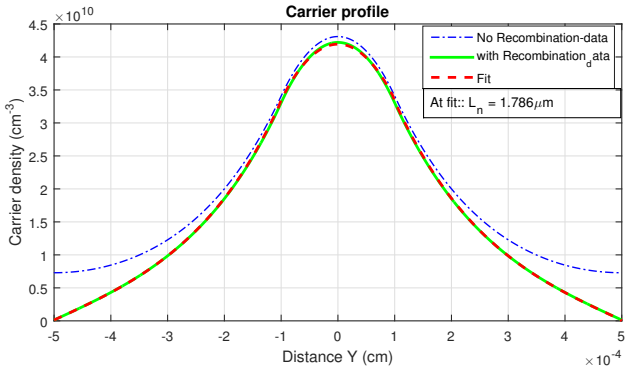

FIGURE 4.2. Numerical data fit with BC. In blue - profile with infinite boundaries. In green - carrier profile when we apply surface recombination and in red dotted is the analytic fit.

Figure 4.2 shows the results of our numerically fitted data. In order to really understand and simulate the effect of surface recombination, we used a relatively longer carrier lifetime (i.e $\tau = 10^{-7}$s) in order to allow carriers diffusion to the boundaries as in blue curve. Now the effect of surface recombination can be clearly seen as in green curve. On fitting the data with surface recombination, we were able to extract the diffusion length $L_n = 1.786\mu m$ nearly similar to the set value of $L_n = 1.799\mu m$. set in the simulation with D = 0.32375.

4.2 2D Numeric Data fitting

As the case with 1D discuses in the section above, here we also made the numerical simulation in 2D to extract the data to be fitted. As we saw in subsection 3.2.1, in order to fit the data in 2D, one need to transform the data from Cartesian coordinates into polar coordinate system so that we can be able to get the radial diffusion length. We saw that the solution of the polar coordinate that can fit our model, is equation 4.9. This solution can only fit the data without surface recombination. If one want to fit the data taking into account the effect of surface recombination, the equation

4.10 can be used. In our case we made the fit on the data without surface recombination effect and we used equation 4.9 to extract the value of the diffusion length.

$$n(r) = A_1 \exp\left(\frac{-r}{L_n}\right) + cst \tag{4.9}$$

and

$$n(r) = \frac{D}{s_n} A_1 \exp\left(\frac{-r}{L_n}\right) + cst \tag{4.10}$$

where r is the radial distance and A_1, A_2 are fitting coefficients. L_n is the diffusion length to be extracted and cst is a constant.

Results and discussion

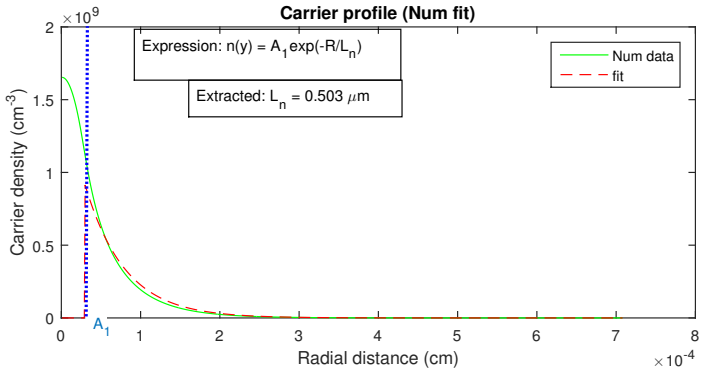

FIGURE 4.3. Numerical data fit 2D. Green - numeric data, red dotted - analytic fit

Figure 4.3 shows carrier profile in 2D. In green is the numeric data profile and red dotted shows the fitting using the solution of polar coordinate system, equation 4.9. Note, the fitting was made from the marked point A' to r = 8×10^{-4}cm. This was because this region showed a good carrier profile and since in our expression we didn't include the carrier generation term, it was wise to just fit the region for carrier diffusion only. Moreover we saw in the previous sections that for a homogeneous material, we can obtain similar results by fitting a region other than the entire profile of the study material and get similar results. Therefore on fit, we were able to extract the value of the diffusion length $L_n = 0.50\mu m$. With fitting accuracy errors and approximations, this value is close to the to the set value of $L_n = 0.56\mu m$ used in our simulation.

4.3 Applying the model to fit Experimental data

Having worked on our numerically extracted data, and knowing that we can use our analytic expressions to successful extract the diffusion length, we then analyzed real experimental data. The data which we worked on was one of the luminescence experiments carried out at IRDEP

characterization laboratory on III-V absorber material (InGaAsP/GaAsP, multi-quantum wells) by Dac Trung Nguyen. Our task was to treat this data with our analytic model to extract the value of the diffusion length.

Results and discussion

Figure 4.4(a) shows the raw experimental data in Cartesian coordinate (in pixels), fig 4.4(b) is the map transformed into polar coordinates system and fig 4.4(c) is the carrier profile (green) with the analytic fit (red dotted). Since the experimental data was in Cartesian coordinates, we needed to transform the data into polar coordinate system such that we can use the analytic solution,equation 4.9 in our model to fit the data and extract the diffusion length.
On fit, we used the analytic expression 4.9, we were able to extract the value of the diffusion length $L_n = 8.47\mu m$. This value is feasible for III-V absorber material.
To be more precise, at IRDEP, in the group I worked with, they also work on the lateral carrier diffusion length in several PV absorbers.Therefore I hope this model will be useful to find its application in extracting the diffusion length from the experimentally obtained data.

(a)

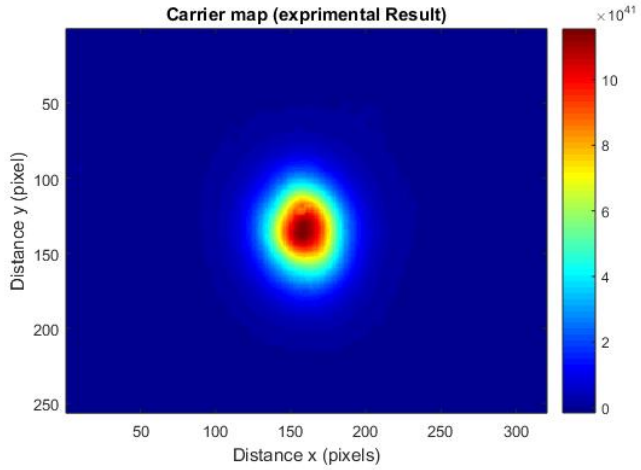

(b)

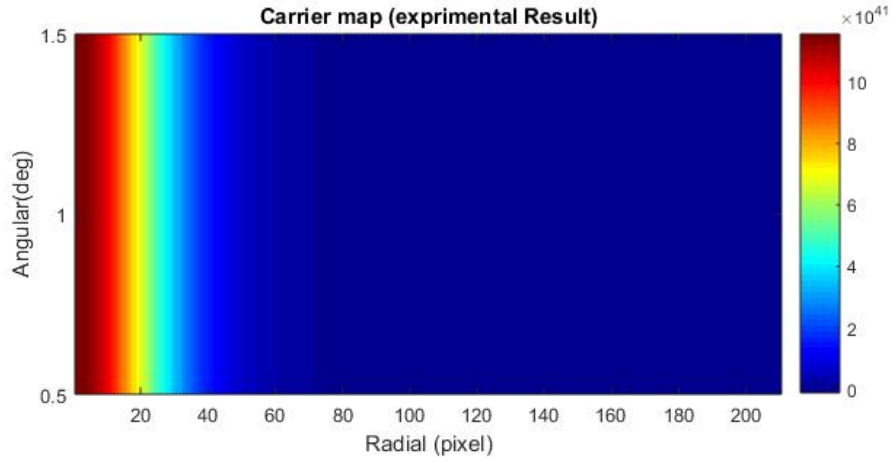

(c)

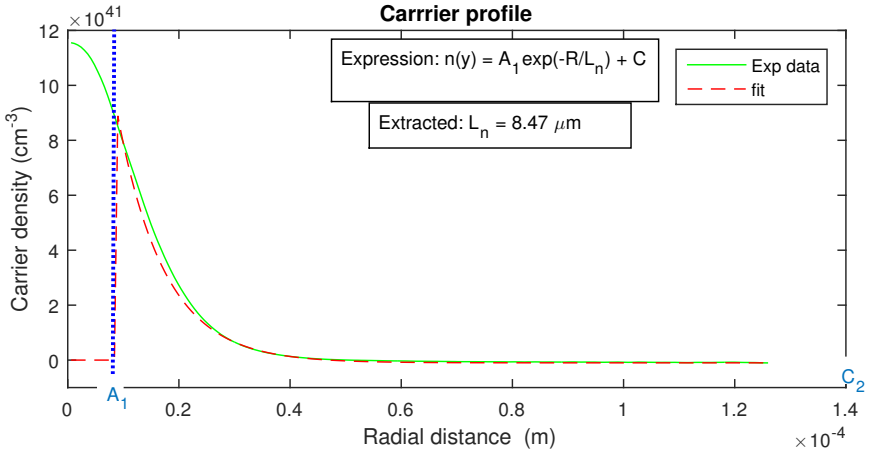

FIGURE 4.4. (a) Carrier map in Cartesian coordinates (b) Map as transformed in Polar coordinates system (c) Carrier profile with fit(in red dotted)

CHAPTER 5

CONCLUSION AND PROSPECTIVE

5.1 Conclusions

First, we have successfully shown that microscopic spatial defects have a profound impact on the global performance of thin film solar cells. Chapter (3) was dedicated to study the effects of defect size, defect recombination rate and surface recombination. In all cases we found out that the material performance is altered greatly by these effects. Therefore care must be taken to model these defects and surface recombination to help the understanding and the characterization tools in order to increase the PV performance.
In chapter five we have shown that it is possible to extract transport properties i.e the diffusion length or(and) surface recombination velocity through fitting the experimentally obtained data using the analytic solution of the diffusion equation. We also found that when extracting transport properties (e.g diffusion length) from the luminescence experiment data, for a homogeneous system, it's possible to extract them by fitting a specific region instead of fitting the whole spectrum which is not a straight forward process. We also shown that we can extract the transport properties around the defect area, if we a dealing with inhomogeneous materials.
Lastly we have shown that mathematical/numerical modeling is a very promising, versatile,and fast characterization technique that provides insight into the spatial quality of PV materials without being affected by experimentally induced defects, or by temperature variations upon illumination. With these features we are confident that it will find wide applications in research and also in the photovoltaic and microelectronic industries.

5.2 Prospective

This study has paved a way to two main prospective: 1. The study was limited to two dimension, we propose also to carry out the same work in 3D.. We used the simplest case to study the lateral diffusion in the bulk, therefore we didn't consider effect of carrier transport in the depth(drift and diffusion). A more complete study of the transport properties and the respective coefficients is still needed. Moreover We based our study on mono-crystalline materials due to limited time and lack of software to model poly-crystalline materials. Therefore we recommend future model to study poly-crystalline materials.
2.From subsection 2.4.1.1 we discussed about generalized Planck's law which describe the emission of luminescence radiation $\Delta\mu = \epsilon_{fn} - \epsilon_{fp} \neq 0$ in equation 5.1 (a phenomenon known as quasi fermi level splitting), where $\Delta\mu = \epsilon_{fn} - \epsilon_{fp}$ is the quasi fermi level.

$$J_n = \frac{1}{4\pi^2\hbar^3c^2}\frac{a(E)E^2}{\exp(\frac{E-\Delta\mu}{K_BT})-1} \tag{5.1}$$

The current is linked to the spatial variation of the quasi fermi level as;

$$\overrightarrow{j_n} = \frac{\sigma_e}{e}\overrightarrow{\nabla}\epsilon_{fn} \tag{5.2}$$

where σ_e is the electrical conductivity.
As we can now access experimentally to this quantity($\Delta\mu$),the idea will be to treat transport equation based on these relations closer to the luminescence description. One can also take into account the carrier temperature. We believe that further studies could allow accessing to a complete set of transport properties(i.e electrical and thermal conductivity, mobility, etc).

APPENDIX A

APPENDIX A

A.1 Thin film solar cells

Photovoltaic is a multidisciplinary field that requires an understanding of physics, chemistry, material science and production technologies. People who dedicated their life in this field have three common objectives (1) to improve the conversion efficiency of the devices, (2) to develop processes that will allow for lower production costs, (3) to ensure that module performances will be maintained for several decades in outdoor conditions, thereby providing much more energy than used in production. Of recent people have realized that thin film (TF) technilogy is a way to achieve the above objectives. TF technologies use small amounts of active materials and can be manufactured at a lower full cost than c-Si. They have short energy pay-back times (i.e. <1yr in southern Europe) despite their lower efficiency, good stability and lifetimes comparable to c-Si modules.

Thin-film photovoltaics has been defined in different context.The definition from [2],Thin-film (TF) photovoltaics (PV) is based on large-area planar devices where conversion of light into electricity takes place in a thin multilayer structure only a few micrometres thick. Thin films may encompass a considerable thickness range, varying from a few nanometers to tens of micrometers and could also be defined in terms of the production processes rather than by thickness.
On the physics point view Thin film defined from other conventional semiconductors such as crystalline silicon which has an indirect band gap with weak absorption,Thin films have a direct band gap hence strong absorption properties.

A.1.1 Thin film absorber materials

Conventionally, photovoltaic materials use inorganic semiconductors. The semiconductors of interest allow the formation of charge-carrier separating junctions. The junction can be either a homojunction (like in Si) or a heterojunction with other materials to collect the excess carriers when exposed to light. In principle, a large number of semiconductor materials are eligible, but only a few of them are of sufficient interest. Ideally, the absorber material of an efficient terrestrial solar cell should be a semiconductor with a bandgap of 1-1.5 eV with a high solar optical absorption in the wavelength region of 350-1000 nm, a high quantum yield for the excited carriers, a long diffusion length low recombination velocity. If all these constraints are satisfied and the basic material is widely available, the material allows in principle the manufacturing of a thin-film solar cell device. From the point of view of processing, manufacturing and reproducibility, elemental semiconductors provide a simple and straightforward approach to manufacture thin-film solar cells. Amongst TF PV devices are amorphous-silicon (a-Si), multi-junction amorphous-silicon/microcrystalline-silicon ($a-Si/\mu c-Si$), chalcopyrite $Cu(In_x,Ga_{(1-x))}(Se,S)_2(CIGS)$, and cadmium telluride solar cells (CdTe), as well as dye-sensitised solar cells (DSSC), organic solar cells (OSC) and as the youngest type of TF solar cells, the so-called perovskite solar cells.
III-V compound materials like GaAs, InP and their derived alloys and compounds, which most often have a direct bandgap character, are ideal for photovoltaic applications, but are far too expensive for large-scale commercial applications, because of the high cost of the necessary precursors for the deposition and the deposition systems itself.
More appealing from the point of view of ease of processability and cost of material and deposition are the 'II-VI compound materials' like CdTe or variations on this like $CuInSe_2$. The interest in these materials for thin-film solar cell manufacturing is essentially based on two elements. Because of the chemical structure of these materials the internal (grain boundaries, interfaces) and external surfaces are intrinsically well passivated and characterized by a low recombination velocity for excess carriers. The low recombination activity at the grain boundaries allows high solar cell efficiencies even when the material is polycrystalline with grain sizes in the order of only a few μm. This is to be contrasted with crystalline Si where grain boundaries are normally characterized by a high recombination velocity. Moreover, the polycrystallinity allows a large number of substrates (glass, steel foil, . . .) and is compatible with low-cost temperature deposition techniques, as there is no need for epitaxial growth or high temperatures to obtain large grain sizes. A second important property is the possibility to tailor the bandgap e.g. replacing Se by S in $CuInSe_2$ results in a material with a higher bandgap. This property allows one to build in bandgap gradients aiding the collection of excess carriers and, ultimately, could even be used to develop multijunction solar cells.

A new record for thin film solar cell efficiency of 22.6% has been achieved by ZSW[1] (Zentrum fur Sonnenenergie- und Wasserstoff-Forschung - or Center for Solar Energy and Hydrogen Research -Baden-Wurttemberg) in Stuttgart, Germany. ZSW's latest record-setting cell has an area of about $0.5cm^2$ using CIGS technology[21] beating the the Japanese firm Solar Frontier[2], which exceeded 22.3% efficiency using CIS technology[12]. The world conversion efficiency record of 22.1% for cadmium-telluride solar photovoltaic cells has been achieved by First Solar[3][7]. A world record initial efficiency of 14.8% has been achieved in tandem thin-film silicon solar cells[13]. The youngest TF solar cells, (perovskites) have shown fast improvement with a record power-conversion efficiency of 21.1% and 18% after 250 hours under operational conditions[8].

Despite more than 30 years of research invested in each of the thin-film solar cell technologies considered here, a large series of questions has still to be answered. The need for more 'know-why' in addition to the available 'know-how' is urged by the responsibility of scientists toward a steadily growing industry and toward a world in need for clean energy. Fortunately, more and more specialists for sophisticated physical and chemical analysis methods enter the field and help improving our common understanding as well as improving our technology. The most satisfying answers always will arise from a combination of a solid understanding of the photovoltaic principles with the results from various methods analyzing the electronic, chemical, and structural properties of all the layers and interfaces in the device.

[1]ZSW: https://www.zsw-bw.de/en.html
[2]Solar Frontier: http://www.solar-frontier.com/eng/
[3]First Solar: http://www.firstsolar.com

APPENDIX B

APPENDIX B

Here we present the analytic solution in one dimension used in our model. We first solve the general solution. In our model we first studied the case with infinite boundary conditions, the solution for this particular case is provided, the proceeding solutions of our case studies, that is with boundary conditions and the effect of grain boundaries in the bulk are also given.

B.1 One dimension

From

$$D\bigtriangledown^2 n(y) - \frac{n(y)}{\tau} - G_0(y) = 0 \tag{B.1}$$

Homogeneous solution
let

$$n(y) = \exp(\lambda y) \tag{B.2}$$

$$n''(y) = \lambda^2 \exp(\lambda y) \tag{B.3}$$

$$\lambda^2 \exp(\lambda y) - \frac{n(y)}{\tau D}\exp(\lambda y) = 0 \Rightarrow \lambda = \pm\frac{1}{\sqrt{\tau D}} = \frac{1}{L_n}. \tag{B.4}$$

$$n(y) = C_1 \exp\left(\frac{y}{L_n}\right) + C_2 \exp\left(\frac{-y}{L_n}\right) \tag{B.5}$$

particular solution.

$$n(y) = A\frac{G_0}{D}$$

$$n(y) = -\frac{AG_0}{\tau D^2} + \frac{G_0}{D} = 0$$
$$A = \tau D$$

$$n(y) = L_n^2 \frac{G_0}{D} \tag{B.6}$$

Therefore the general solution for equation B.1 is;

$$n(y) = C_1 \exp\left(\frac{y}{L_n}\right) + C_2 \exp\left(\frac{-y}{L_n}\right) + L_n^2 \frac{G_0}{D} \tag{B.7}$$

B.1.1 With no surface recombination

In our model with infinity boundary condition, we have three expression, in the three different regions.

$$n(y) = A_1 \exp\left(\frac{y}{L_n}\right) \tag{B.8}$$

$$n(y) = B_1 \exp\left(\frac{y}{L_n}\right) + B_2 \exp\left(\frac{-y}{L_n}\right) + L_n^2 \frac{G_0}{D} \tag{B.9}$$

$$n(y) = C_2 \exp\left(\frac{-y}{L_n}\right) \tag{B.10}$$

Since these equations must be continuous; we can include the continuity conditions in order to solve for the coefficients;

$$A_1 \exp\left(\frac{y_1}{L_n}\right) = B_1 \exp\left(\frac{y_1}{L_n}\right) + B_2 \exp\left(\frac{-y_1}{L_n}\right) + g_0 \longleftrightarrow g_0 = L_n^2 \frac{G_0}{D} \tag{B.11}$$

$$A_1 \exp\left(\frac{y_1}{L_n}\right) = B_1 \exp\left(\frac{y_1}{L_n}\right) - B_2 \exp\left(\frac{-y_1}{L_n}\right) + 0 \tag{B.12}$$
$$2B_2 \exp\left(\frac{-y_1}{L_n}\right) = -g_0$$

$$B_2 = -\frac{g_0}{2} \exp\left(\frac{-y_1}{L_n}\right) \tag{B.13}$$

$$A_1 = B_1 - B_2 \exp\left(\frac{-2y_1}{L_n}\right) \tag{B.14}$$

$$C_2 \exp\left(\frac{y_2}{L_n}\right) = B_1 \exp\left(\frac{y_2}{L_n}\right) + B_2 \exp\left(\frac{-y_2}{L_n}\right) + g_0 \tag{B.15}$$

(B.16) $$C_2 \exp\left(\frac{y_2}{L_n}\right) = B_1 \exp\left(\frac{y_2}{L_n}\right) - B_2 \exp\left(\frac{-y_2}{L_n}\right) + 0$$

$$2B_1 \exp\left(\frac{-y_2}{L_n}\right) = -g_0$$

(B.17) $$B_1 = -\frac{g_0}{2} \exp\left(\frac{-y_2}{L_n}\right)$$

(B.18) $$C_2 = B_2 - B_1 \exp\left(\frac{-2y_2}{L_n}\right)$$

B.1.2 Applying surface recombination

Solution of equation B.1 with non infinity Boundaries. i.e if we now take into consideration the surface recombination velocity.

(B.19) $$n(y) = A_1 \exp\left(\frac{y_2}{L_n}\right) + A_2 \exp\left(\frac{-y_2}{L_n}\right)$$

(B.20) $$n(y) = B_1 \exp\left(\frac{y_2}{L_n}\right) + B_2 \exp\left(\frac{-y_2}{L_n}\right) + g_0.$$

(B.21) $$n(y) = C_1 \exp\left(\frac{y_2}{L_n}\right) + C_2 \exp\left(\frac{-y_2}{L_n}\right)$$

at y_0

(B.22) $$\frac{\partial n}{\partial y} = -\frac{S}{D} n(y_0) = \frac{A_1}{L_n} \exp\left(\frac{y_0}{L_n}\right) - \frac{A_2}{L_n} \exp\left(\frac{-y_0}{L_n}\right) = -\frac{S}{D}\left(A_1 \exp\left(\frac{y_0}{L_n}\right) + A_2 \exp\left(\frac{-y_0}{L_n}\right)\right)$$

were S is the surface recombination velocity.

(B.23) $$A_2 = A_1 \exp\left(\frac{2y_0}{L_n}\right) \frac{\left(1 - \frac{SL_n}{D}\right)}{\left(1 + \frac{SL_n}{D}\right)} = \frac{-w}{x} A_1 \exp\left(\frac{2y_O}{L_n}\right)$$

with $x = \left(\frac{SL_n}{D} + 1\right)$ and $w = \left(\frac{SL_n}{D} - 1\right)$ at y_1

(B.24) $$2A_2 \exp\left(\frac{-y_1}{L_n}\right) = 2B_2 \exp\left(\frac{-y_1}{L_n}\right) + g_0$$

(B.25) $$B_2 = A_2 - \frac{g_0}{2} \exp\left(\frac{y_1}{L_n}\right)$$

Considering the continuity condition around y_1, taking the derivatives in A and B, we have,

(B.26) $$A_1 \exp\left(\frac{y_1}{L_n}\right) - A_2 \exp\left(\frac{-y_1}{L_n}\right) = B_1 \exp\left(\frac{y_1}{L_n}\right) - B_2 \exp\left(\frac{-y_1}{L_n}\right)$$

$$A_1 = B_1 - B_2 \exp\left(\frac{-2y_1}{L_n}\right) + A_2 \exp\left(\frac{-2y_1}{L_n}\right)$$

Using equations B.23 and B.25 we get

$$A_1 = B_1 + \frac{g_0}{2} \exp\left(\frac{-y_1}{L_n}\right) \tag{B.27}$$

at y_3

$$\frac{\partial n}{\partial y} = \frac{S}{D} n(y_3) = \frac{C_1}{L_n} \exp\left(\frac{y_3}{L_n}\right) - \frac{C_2}{L_n} \exp\left(\frac{-y_3}{L_n}\right) = \frac{S}{D}\left(C_1 \exp\left(\frac{y_3}{L_n}\right) + C_2 \exp\left(\frac{-y_3}{L_n}\right)\right) \tag{B.28}$$

$$C_1 = -\frac{w}{x} C_2 \exp\left(\frac{-2y_3}{L_n}\right) \tag{B.29}$$

at y_2

$$2B_1 \exp\left(\frac{y_2}{L_n}\right) + g_0 = 2C_1 \exp\left(\frac{y_2}{L_n}\right)$$

$$B_1 = C_1 - \frac{g_0}{2} \exp\left(\frac{-y_2}{L_n}\right) \tag{B.30}$$

Considering the continuity condition around y_2, taking the derivatives in B and C, we have,

$$C_1 \exp\left(\frac{y_2}{L_n}\right) - C_2 \exp\left(\frac{-y_2}{L_n}\right) = B_1 \exp\left(\frac{y_2}{L_n}\right) - B_2 \exp\left(\frac{-y_2}{L_n}\right) \tag{B.31}$$

and using equations B.23 to B.30 we can find;

$$C_2 = \frac{g_0}{2} \frac{wp}{x} \left(\exp\left(\frac{2y_0}{L_n} - \frac{y_2}{L_n}\right) - \exp\left(\frac{2y_0}{L_n} - \frac{y_1}{L_n}\right)\right) + \frac{g_0}{2p} \left(\exp\left(\frac{y_2}{L_n} - \frac{y_1}{L_n}\right)\right) \tag{B.32}$$

with $p = 1 - \frac{w^2}{x^2} \exp\left(\frac{-2y_3}{L_n} + \frac{2y_0}{L_n}\right)$

B.1.3 Creating grain boundaries

Here for regions were modeled (reference) and the solutions are

$$n(y) = A_1 \exp\left(\frac{y}{L_1}\right) \tag{B.33}$$

$$n(y) = B_1 \exp\left(\frac{y}{L_1}\right) + B_2 \exp\left(\frac{-y}{L_1}\right) + g_0. \tag{B.34}$$

$$n(y) = C_1 \exp\left(\frac{y}{L_2}\right) + C_2 \exp\left(\frac{-y}{L_2}\right) \tag{B.35}$$

$$n(y) = D_1 \exp\left(\frac{-y}{L_1}\right) \tag{B.36}$$

at y_1

$$A_1 \exp\left(\frac{y_1}{L_1}\right) = B_1 \exp\left(\frac{y_1}{L_1}\right) + B_2 \exp\left(\frac{-y_1}{L_1}\right) + g_0 \tag{B.37}$$

$$A_1 \exp\left(\frac{y_1}{L_1}\right) = B_1 \exp\left(\frac{y_1}{L_1}\right) - B_2 \exp\left(\frac{-y_1}{L_1}\right) + 0 \tag{B.38}$$

$$A_1 = B_1 - B_2 \exp\left(\frac{-2y_1}{L_1}\right) \tag{B.39}$$

$$B_2 = -\frac{g_0}{2} \exp\left(\frac{y_1}{L_1}\right) \tag{B.40}$$

at y_2

$$B_1 \exp\left(\frac{y_1}{L_1}\right) + B_2 \exp\left(\frac{-y_1}{L_1}\right) + g_0 = C_1 \exp\left(\frac{y_2}{L_2}\right) + C_2 \exp\left(\frac{-y_2}{L_2}\right) \tag{B.41}$$

$$\frac{B_1}{L_1} \exp\left(\frac{y_1}{L_1}\right) - \frac{B_2}{L_1} \exp\left(\frac{-y_1}{L_1}\right) + 0 = \frac{C_1}{L_2} \exp\left(\frac{y_2}{L_2}\right) - \frac{C_2}{L_2} \exp\left(\frac{-y_2}{L_2}\right) \tag{B.42}$$

from equations B.41 and B.42 we get;

$$B_1 = C_1 \exp\left(\frac{y_2}{L_2} - \frac{y_2}{L_1}\right) + C_2 \exp\left(\frac{-y_2}{L_1} - \frac{y_2}{L_1}\right) - B_2 \exp\left(\frac{-2y_2}{L_1}\right) - g_0 \exp\left(\frac{-y2}{L_1}\right) \tag{B.43}$$

at y_3

$$C_1 \exp\left(\frac{y_3}{L_2}\right) + C_2 \exp\left(\frac{-y_3}{L_2}\right) = D_2 \exp\left(\frac{-y_3}{L_1}\right) \tag{B.44}$$

$$\frac{C_1}{L_2} \exp\left(\frac{y_3}{L_2}\right) - \frac{C_2}{L_2} \exp\left(\frac{-y_3}{L_2}\right) = \frac{D_2}{L_1} \exp\left(\frac{-y_3}{L_1}\right) \tag{B.45}$$

which gives;

$$D_2 = C_1 \exp\left(\frac{y_3}{L_2} + \frac{y_3}{L_1}\right) + C_2 \exp\left(\frac{y_3}{L_1} - \frac{y_3}{L_2}\right) \tag{B.46}$$

$$C_1 = C_2 \exp\left(\frac{-2y_3}{L_2}\right) \left(\frac{\frac{L_1}{L_2} - 1}{\frac{L_1}{L_2} + 1}\right) \tag{B.47}$$

Using equations B.42 to B.45 we get;

$$C_2 = \Gamma(2B_2 \exp\left(\frac{-y_2}{L_1} + \frac{y_2}{L_2}\right) + g_0 \exp\left(\frac{y_2}{L_2}\right) \tag{B.48}$$

were; $\Gamma = \frac{\frac{L_1}{L_2}+1}{\left(\frac{L_1}{L_2}+1\right)^2 - \left(\frac{L_1}{L_2}-1\right)^2 \exp\left(\frac{-2y_3}{L_2} + \frac{2y_2}{L_2}\right)}$

APPENDIX C

APPENDIX C

Because our aim was to study the spatial effects, it was a prerequisite to find the analytic expression that can be used to fit numeric results. The MATLAB toolbox app used to model our work was specifically built to compute 2D differential equation problems, however it can also be adjusted to solve the 1D and 3D problems. The 2D analytic solution is not soo trivial problem and to get the physical meaning of our study it was not a neccessity to present the exact solution in 2D. Instead we needed to transform our solution into polar coordinate system in order to model the radial decay which rather best give the physical meaning of spatial modeling.

C.1 Solution in polar coordinate form

The Laplacian in equation B.1 can be transformed into polar coordinate system as;

$$\frac{1}{r}\frac{\partial(Dr\frac{\partial n(r)}{\partial r})}{\partial r}+\frac{1}{r^2}\frac{\partial(D\frac{\partial n(r)}{\partial \theta})}{\partial \theta}-\frac{n(r)}{\tau}+G_0(r)=0 \tag{C.1}$$

Since the problem is axis-symmetric; then $\frac{\partial n(r)}{\partial \theta}=0$ equation C.1 becomes;

$$\frac{\partial(Dr\frac{\partial n(r)}{\partial r})}{\partial r}-r\frac{n(r)}{\tau}+G_0(r)=0 \tag{C.2}$$

which can be written as

$$\frac{\partial^2 n}{\partial r^2}+\frac{1}{r}\frac{\partial n}{\partial r}-\frac{n(r)}{\tau D}+\frac{G_0(r)}{D}=0 \tag{C.3}$$

Particular solution, i e

$$\frac{\partial^2 n}{\partial r^2}+\frac{1}{r}\frac{\partial n}{\partial r}-\frac{n(r)}{\tau D}=0 \tag{C.4}$$

For the above expression to be satisfied, at-least two of the three terms must balance each other in order of magnitude with the term left out having smaller or equal order of magnitude but not greater. If we consider the first and second terms, it means

$$\frac{\partial n}{\partial r} \approx \frac{1}{r} \Rightarrow n(r) \approx \ln(r) \tag{C.5}$$

which is big compared to the first and second term.

Now taking the second and third terms

$$n(r) \approx C_1 \exp(\frac{r^2}{2\tau D}) \tag{C.6}$$

This also outweighs the other two terms; Now the only left trial is balancing the third and first terms. This gives;

$$n(r) \approx C_1 \exp(\frac{-r}{\sqrt{\tau D}}) \tag{C.7}$$

This makes the second term insignificant and drop out. Hence the only feasible leading behavior of eqtn (C.4) and since $\sqrt{\tau D} = L_n$ is;

$$n(r) \approx C_1 \exp(\frac{-r}{L_n}) \tag{C.8}$$

Here C_1 is an integration constant, r is the radial distance and L_n is minority carrier diffusion length.

BIBLIOGRAPHY

[1] K. J. BATHE AND E. L. WILSON, *Numerical Methods in Finite Element Analysis.*, Prentice-Hall, Inc, 1976.

[2] M. BOKALIC AND M. TOPIC, *Spatially Resolved Characterization in Thin Film Photovoltaics*, Springer Briefs in Electrical and Computer Engineering, 2014.

[3] A. R. D. PAGET, F. CADIZ, *Imaging ambipolar diffusion of photocarriers in gaas thin films*, applied physics, 111 (2012), pp. 1–5.

[4] T. D. DAN GROIS, IGOR SHCHERBACK AND O. YADID-PECHT, *Theoretical approach to cmos aps psf and mtf modeling,Äîevaluation*, IEEE sensors journal, 6 (2006), pp. 118–124.

[5] T. K. DANIEL ABOU-RAS AND U. RAU, *Advanced Characterization Techniques for Thin Film Solar Cells*, Wiley-VCH Verlag GmbH, 2010.

[6] A. H. S. KLAUS JAGER, OLINDO ISABELLA, *Solar Energy Fundamentals, Technology, and Systems*, Delft, the Netherlands, 2014.

[7] H. LINDON, *First Solar Achieves New Conversion Efficiency World Record For CdTe Solar PV Cells*, http://cleantechnica.com/2016/02/23/first-solar-achieves-new-conversion-efficiency-world-record-cdte-solar-pv-cells/, 2016.

[8] J.-Y. S. K. D. MICHAEL SALIBA, TAISUKE MATSUI, *Cesium-containing triple cation perovskite solar cells: improved stability, reproducibility and high efficiency,Ä†*, Royal society of Chemistry, 9 (2016), pp. 1853–2160.

[9] M. C. S. J. A. G. PAUL GUNDEL, FRIEDEMANN D. HEINZ AND W. WARTA, *Quantitative carrier lifetime measurement with micron resolution*, JOURNAL OF APPLIED PHYSICS, 801 (2010), pp. 1–7.

[10] D. S. PHILIPPS AND W. WARMUTH, *Photovoltaics Report*, Fraunhofer Institute for Solar Energy Systems, ISE, 2016.

[11] J. POORTMANS AND V. ARKHIPOV, *Thin Film Solar Cells Fabrication, Characterization and Applications*, John Wiley & sons, 2006.

[12] G. R. PRABHU, *World Record Thin-Film Solar Cell Efficiency of 22.3% achieved by solar frontier*, http://www.renewindians.com/2015/12/world-record-thin-film-solar-cell.html, 2015.

[13] PROF. MIRO ZEMAN AND W. BATIST, *Towards record thin-film silicon-based solar cells*, Delft Energy Initiative, 2015.

[14] L. SCHWARTFEGER AND A. MILLER, *Environmental Aspects of Photovoltaic Solar Power*, EEA Conference 2015, 2015.

[15] W. SHOCKLEY AND H. J. QUEISSER, *Detailed balance limit of efficiency of p-n junction solar cells**, Applied Physics, 32 (1961), pp. 510–519.

[16] W. SHOCKLEY AND W. READ, *Statistics of the recombinations of holes and electrons*, Physical Review, 87 (1952), pp. 510–519.

[17] L. SIGERLIND, *Applied Finite Element Analysis*, John Wiley and Sons, Inc, 1976.

[18] R. A. SMITH, *Semiconductors*, Cambridge University press, 1978.

[19] S. S.RAO, *The Finite Element Method in Engineering*, Pergamon Press, 1989.

[20] R. A. B. T. TRUPKE AND W. WARTA, *Photoluminescence imaging of silicon wafers*, Applied physics letter, 89 (2006), pp. 2–4.

[21] S. TODAY, *ZSW regains thin-film solar cell efficiency record with 22.6% CIGS PV cell*, Juno Publishing and Media Solutions Ltd:, 2016.

[22] P. WURFEL AND U. WURFEL, *Physics of solar cells*, WILEY VCH, 2009.